



This is a repository copy of *Achieving emission reduction through the utilisation of local low-grade heat sources in district heating networks*.

White Rose Research Online URL for this paper:

<https://eprints.whiterose.ac.uk/207360/>

Version: Published Version

Article:

Cowley, T., Hutton, T., Hammond, J. et al. (1 more author) (2024) Achieving emission reduction through the utilisation of local low-grade heat sources in district heating networks. *Applied Thermal Engineering*, 242. 122381. ISSN 1359-4311

<https://doi.org/10.1016/j.applthermaleng.2024.122381>

Reuse

This article is distributed under the terms of the Creative Commons Attribution (CC BY) licence. This licence allows you to distribute, remix, tweak, and build upon the work, even commercially, as long as you credit the authors for the original work. More information and the full terms of the licence here:

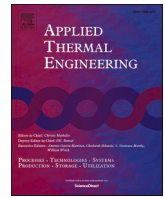
<https://creativecommons.org/licenses/>

Takedown

If you consider content in White Rose Research Online to be in breach of UK law, please notify us by emailing eprints@whiterose.ac.uk including the URL of the record and the reason for the withdrawal request.



eprints@whiterose.ac.uk
<https://eprints.whiterose.ac.uk/>



Research Paper

Achieving emission reduction through the utilisation of local low-grade heat sources in district heating networks

Thomas Cowley, Timothy Huty, Joseph Hammond, Solomon Brown *

Department of Chemical and Biological Engineering, University of Sheffield, Sheffield S1 3JD, United Kingdom

ARTICLE INFO

Keywords:

Energy
Heat decarbonisation
District heat networks
Agent-based modelling
Mine water

ABSTRACT

Decarbonising heat provision is paramount in the global shift towards sustainable energy, and waste heat utilisation presents a transformative opportunity, especially in areas of industrial activity. Accordingly, this study examines the performance of District Heating Networks (DHNs) integrated with unconventional heat sources, specifically mine water and industrial waste heat, aiming to derive a comprehensive understanding of the techno-economic and environmental implications of various DHN configurations. To this end a refined network dynamics simulation model has been developed and employed to evaluate the cost and performance of several network size and heat source combinations, with a case study carried out for Barnsley, UK. Results indicate that large networks can achieve an average thermal efficiency of approximately 87%. Networks utilising mine water have a Levelized Cost of Heat (LCOH) in the range 11.6 – 11.9 p/kWh; introducing industrial waste heat reduces this to 10.6 – 10.7 p/kWh. Additionally, waste heat integration lowers the carbon factor of the supplied heat to 0.05 kgCO₂/kWh. Transitioning from boilers to district heating in the region covered by the case study networks showed a marginal emission reduction ranging from 44.76% to 83.46%. The gas price at which these networks achieve economic viability varies from 8.6 to 8.8 p/kWh. In conclusion, the DHNs proposed, especially when augmented with industrial waste heat, emerge as a promising solution for areas like Barnsley in their pursuit of sustainable heating. These findings are pivotal for policymakers and local governing bodies as the UK gears up to meet its 2050 net-zero ambitions.

1. Introduction

It is widely recognised that carbon dioxide significantly contributes to climate change, driving leading economies to reduce carbon emissions [1]. The UK, amongst others, has pledged to reach net-zero greenhouse gas emissions (GHG) by 2050 [2]. While the UK has made progress towards decarbonisation of its electricity grid, the heating sector, responsible for 23 % of all UK emissions, remains a challenging target [3–4]. Given this scenario, district heating networks (DHNs) are gaining interest, intending to connect large sets of customers to low-carbon heat generation systems [5–6], especially at a community or district level, with typical sizes of up to 10's MW at peak demand [7]. Yet, they compete with other low-carbon technologies like air source heat pump (ASHP) or ground source heat pump (GSHP) [8–9], whose implementation is slowed by the perceived skill gap in design and installation, and associated costs [10–11]. Across Europe, the proliferation of DHNs underscores their potential as enablers of low-carbon heat generation. This study shows that the majority of the successful systems

leverage local heat demand and access to generation sources [13]. As the UK considers the adoption of DHNs, it's essential to incorporate these findings, informed by the European experience and compare them to alternative heating options [12]. Currently, the utilisation of heat networks in the UK is limited, with only 2 % of the total heat demand being met by DHN, indicating minimal experience with this technology in the UK [13].

The adoption of DHN systems in the UK is fraught with challenges; the most significant is their uncertain techno-economic feasibility [14]. While network dynamics models are instrumental in grasping these systems, they frequently simplify techno-economic analysis, like K. Sartor et al. which bases its economics on peak power demand only [15]. Conversely, techno-economic studies do not include any form of network dynamics simulation to accurately obtain results. A vast majority of these models either lack the necessary generality to accurately represent performance across different regions and network sizes, or they are not computationally efficient enough to simulate across an entire year. Work by B. Back et al. simplify their model to only simulate 1 week for each month, stating that this gave 'a number of issues' in the

* Corresponding author.

E-mail address: s.f.brown@sheffield.ac.uk (S. Brown).

<https://doi.org/10.1016/j.applthermaleng.2024.122381>

Received 31 July 2023; Received in revised form 4 December 2023; Accepted 3 January 2024

Available online 13 January 2024

1359-4311/© 2024 The Author(s). Published by Elsevier Ltd. This is an open access article under the CC BY license (<http://creativecommons.org/licenses/by/4.0/>).

Nomenclature**Acronyms**

ASHP	air source heat pump
CAPEX	capital expense
CHP	combined heat and power
COP	coefficient of performance
DC	demand centre
DEC	display energy certificates
DHN	district heating network
GIS	geographic information system
GHG	greenhouse gas
GSHP	ground source heat pump
HIU	heat interface unit
HP	heat pump
LCOH	levelized cost of heat
LP	linear programming
LTC	sum of costs over lifetime
MIDAS	MET office integrated data archive system
NON-DEC	none display energy certificates
NPC	net present cost
O&M	operation and maintenance
OPEX	operating expense
RHPP	renewable heat premium payment
SEAP	sustainable energy action plan

Symbols

C	cost factor, £/MWh
CC	capital cost, £
CC_t	total capital cost, £
CO_{2b}	emissions of boiler, kg
CO_{2bT}	emissions from entire region of boilers, kg
CO_{2gc}	emissions from a generation centre, kg
CO_{2hp}	emissions from a heat pump, kg
CO_{2MR}	marginal reduction in emissions, %
CO_{2p}	emissions from repressuring pump, kg
CO_{2s}	carbon savings, %
CO_{2total}	emissions from the DHN, kg
CSA	cross sectional area of pipe, m^2
c_w	specific heat capacity of water, kJ/kgK
d	burial depth, m
d_{in}	Diameter, mm
E	electricity price, p/kWh
e	error term, kW
E_t	total energy cost, £
F	shape factor, –
f	carbon factor, t/MWh
h_{co}	convection coefficient, $Wm^{-2}K^{-1}$
i	rate of inflation, %
L_p	route length, m

L_T	total network length, m
\dot{m}	mass flowrate, kg/s
Nu	Nusselt number, –
P_{GC}	capacity of plant, kW_{th}
P_{HP}	power consumption of heat pump, kW
P_r	repressuring power, kW
Pr	Prantl number, –
Q	thermal energy, kJ
\dot{Q}	thermal power, kW_{th}
q	flux, Wm^{-2}
r	radius, mm
R	discount factor, –
Re	Reynolds number, –
R_{nom}	nominal discount factor, –
R'	losses per metre of pipe per °K (reciprocal of), $(Wm^{-1}K^{-1})^{-1}$
SA	surface area, m^2
t	time, <i>hours</i>
T	temperature, °C
\hat{T}	boundary temperature, °C
v	flow velocity, ms^{-1}
\dot{V}	volumetric flowrate, m^3s^{-1}
α_{diff}	diffusivity coefficient, m^2s
ΔP	pressure drop, kPa
ϵ_A	absolute roughness, m
ϵ_R	relative roughness, –
μ	friction factor, –
ν	kinematic viscosity, mm^2s^{-1}
ρ_w	density, kgm^{-3}

Subscripts

A	ancillary equipment
B	borehole
b	boiler
BP	main buried pipe
BR	business rates
casing	pipe parameter for casing
DC	demand centre node
GC	generation centre node
HIUM	HIU maintenance
HM	heat meter
HMM	heat meter maintenance
hp	heat pump
IP	internal pipe
N	network
NM	network maintenance
SC	staff maintenance
SS	substation
WH	waste heat

results [16]. Although numerous studies delve into various DHN layouts, many overlook the economic consequences of fluctuating demand, [15 17 18], as well as complex network dynamic functionality such as thermal transience and time delay. The work of E. Guelpa et al analyses the relevance of implementing network dynamics into DHN modelling and the impact of neglecting it. Thermal losses, time delay and thermal transients, were compared in two scenarios; during steady-state operation; and variable control. The most significant phenomenon was the heat lost when there was no flow and the time it took to replenish the water when demand was requested [19]. Keirstead et al.'s work reviewed 219 papers and found that only 44 % of models incorporated geographic information systems (GIS) features, and 58 % used a yearly

temporal scale or greater [20]. In the context of regional heat networks, historical trends have shown that fluctuations in natural gas prices can significantly influence the adoption of DHNs, especially in regions like the UK where natural gas dominates the heating market [15]. Additionally, the increase of heat costs with certain heat generation technologies such as combined heat and power (CHP), as seen in the case of St Bride's Community Centre's efficient modulation during demand fluctuations, further highlights the intricate balance between technology choice and gas pricing, and major increases in demand [6]. This highlights the importance of techno-economic analysis of alternate heat sources, not just CHP if we want to advance the field in the UK, and assessing breakeven gas prices when considering that as networks

expand so does the demand [21–22]. Recent studies highlight the complexities of energy system assessments, especially when balancing economic and environmental concerns [23–15]. Sensitivity analyses reveal the system's susceptibility to changes in fuel and CO₂ quota, cautioning against a narrow focus. A significant insight is the economic feasibility of expanding district heating networks to harness wasted energy. Yet, the research advises in such expansion to try an encompass a well-rounded assessment, including changes in demand and scale [24–25].

Recent advancements in Europe's DHN technology emphasize the evolution towards 4th and 5th-generation networks (4GDH, 5GDH) [26–27–28–29], and are notable for their integration with electricity grids, smart systems, and low-temperature functionality [30–28–26–31]. A specific study highlighted that transitioning the district heating (DH) system to function at lower temperatures can lead to enhanced building efficiency and a notable decrease in reliance on natural gas [29]. The research further indicated that such modernisations can substantially reduce network losses, offering both environmental and operational benefits. Work by P. Ostergaard et al in Aalborg is a prominent example of a network that uses low-temperature geothermal energy, wind turbines with a grid connection, and biomass [32]. It shows independence from natural gas and flexibility to align its production with the demand of the network while also being very economical by taking advantage of electricity price fluctuations. This can help recuperate the high capital costs, often borne by local authorities. To address this user-friendly tools that are flexible enough to be applied to different regions and topological layouts of DHNs while also uncovering complex systems like in Aalborg can break down some of the berries for implementation [33], enabling a broader range of decision-makers to understand the potential of DHN and leverage their local topology [34].

As the UK consider integrating these advancements, understanding these outputs becomes crucial for informed decision-making in DH system adaptations. While low-temperature DHNs have shown adaptability in older European buildings [29], their potential in the UK, remains untapped, highlighting a significant research gap and emphasising the value of this study. Considering Barnsley's older infrastructures, findings indicate that even 70s-era houses can benefit from such DH networks. These networks, with operation temperatures as low as 45 °C for 4GDH [35], permit connection to low-grade heat sources like mine water, in areas like Barnsley with a rich mining history [36–37]. Abandoned coal mines contain groundwater heated by the earth's geothermal gradient and provide an estimated 2.2 million GWh of heat stored below 25 % of UK homes [38–39]. The extracted heat can be utilised for warming nearby homes, with minimal thermal losses due to the proximity to demand [36]. The temperatures of flooded mines typically range between 10 and 20 °C but can reach up to 40 °C [37]. Currently, only a few large schemes, such as Seaham Garden Village, Gateshead, Hebburn, Holburn, and Caerau, are operational [40–41]. The utilisation of these sources within low-temperature networks [35] particularly under the principles of 4th and 5th-generation district heating, presents promising techno-economics and ample opportunities for significant carbon reduction [42–43]. These solutions form an integral part of the broader smart energy systems that encompass integrated systems for electricity, heating, and cooling [27].

Comparative studies underscore the potential of harnessing mine water energy for district heating. While some approaches have shown operational advantages, such as achieving high coefficients of available output, they also encounter challenges like significant energy losses [44]. Delving deeper into geothermal mine water systems, their sustainability, versatility, and reduced carbon footprint stand out, but these benefits also have challenges related to data scarcity, increased pumping costs due to depth, and potential infrastructure modifications [45]. The Laciana Valley's exploration of flooded mines as a source of geothermal heating has shown potential, with certain mines offering significant thermal benefits. However, these ventures face hurdles related to water quality and high initial investments, emphasizing the role of subsidies for profitability [46]. Research into heat extraction from flooded coal

mines suggests that the efficiency of these systems is intricately tied to site-specific geological conditions. The overarching conclusion, though, underscores the potential of using flooded mines for heat storage, with some models indicating long-term benefits [39].

Transitioning to the topic of waste heat, this by-product from industries and data centres presents a promising solution for decarbonizing the heating sector [47–48]. Its potential integration with other heat sources, like mine water, offers an innovative approach yet remains largely uncharted territory. Globally, countries like Sweden have tapped into this potential, with waste heat accounting for a significant portion of their DHN [49]. In the UK, the Bunhill Heat and Power network exemplifies the possibilities, offering both environmental and economic benefits. The system has reduced carbon emissions by 500 tonnes per year as well as providing a minimum 10 % reduction in heating charges for tenants [50]. However, the operational nuances of waste heat in DHNs have challenges, from geographical mismatches between sources and demand areas to the variable availability of waste heat. In areas like Barnsley, waste heat from local industries could bolster DHN efficiency, but a comprehensive techno-economic evaluation remains a gap in the existing literature [51]. Addressing these challenges may hinge on the development of user-friendly tools, promoting easier feasibility assessments and overcoming inherent barriers in DHN implementations [52–53].

Researchers have investigated industrial waste heat and mine water energy independently. However, these studies tend to focus on either waste heat or mine water energy independently, rather than examining the combined effect on DHN performance, economics, and environmental impact. Both A. Matas Escamilla et al. [46] and Antonio Atienza-Márquez et al. [54] emphasize the potential of unconventional sources in district heating. Escamilla and colleagues pinpoint the merits of mine water discharges for heating public buildings, highlighting the open-loop geothermal system as the most efficient. Their findings resonate with the results from the earlier mentioned study on the Laciana Valley, which showed that while the initial investment for geothermal use of mine water is considerable, the environmental and economic returns in the long run make it a viable option. On the other hand, Atienza-Márquez et al. delve into the capabilities of absorption systems in transporting heat within district networks, emphasising how industrial waste heat, similar to that from mine water, can be effectively upgraded and channelled. By integrating the insights from these studies, especially in areas like Barnsley, one can envision a future where the combined benefits of both these low-carbon sources lead to improved environmental, economic, and efficient use of waste heat in district heating and cooling networks.

This study explores the integration of mine water and industrial waste heat into district heating networks, using Barnsley, UK as a focal case study. By incorporating advanced network dynamics and conducting an in-depth techno-economic analysis, the research presents a model that is both adaptable and versatile, suitable for various regional characteristics. The approach taken holistically addresses the changing scale of networks, their economic ramifications, and their emissions impact. The broader implications of this research could steer Barnsley, and similar regions, toward sustainable heating solutions, empowering local authorities, and decision-makers. This offers a unique perspective on heating solutions that align with the UK's ambitious 2050 net-zero GHG emission goals.

The paper is organised as follows: Section 3 describes the construction of the simulation model and its sub-models. Section 4 provides the case study setup and data used as input to the developed model and operational parameters of the heat networks. The results are presented in Section 5, with comprehensive sensitivity analyses to identify and quantify the main techno-economic drivers and implications of different alternatives under different scenarios. Finally, the conclusions drawn from the studies and insights for future work are presented in Section 6. This work aims to measure the effectiveness and feasibility of the potential new DHN in Barnsley to understand the trade-off between cost

and emissions for large-scale mine water heat pumps and how that meets the heat demand in the region, consisting of standalone gas boilers. This will help to answer the following research aims and objectives:

- Develop and refine a network dynamics simulation model accounting for thermal fronts, to accurately capture the performance of DHNs when integrating non-traditional heat sources.
- Investigate the trends and patterns as the network expands and understand the implications of integrating industrial waste heat.
- Quantify the economic benefits and challenges of integrating mine water and industrial waste heat into DHNs, focusing on factors like fuel cost savings, Net Present Costs (NPC), and Levelised Cost of Heat (LCOH).
- Assess the environmental benefits of the proposed DHNs, particularly in terms of emission reductions, and understand the relevance and viability of using low-carbon sources.

2. Methodology

2.1. Overview

The following section describes the developed network dynamics simulation of a DHN. The purpose of the model is to simulate the extraction of mine water heat from unused coal mines, for distribution

via the DHN to various heat demands, both domestic and non-domestic. A high-level overview of the model, which is implemented in AnyLogic simulation software [55], is given in Fig. 1; shown are the data inputs, various sub-models and agents, and modelling outputs, which include both physical and techno-economic metrics.

The network simulation employs an agent-based approach; thus, the behaviour of the model is determined by the actions of the individual agents situated at heat network nodes, rather than employing any form of top-down control or optimisation. For instance, demand agents observe the flow temperature at their location, and adjust the flow at their own node to attempt to meet demand; these control actions can affect flow and temperature throughout the network, leading to feedback effects.

Table 1 provides an overview of all agents included in the model. Primary agents of the model are nodes (demand centres, generation centres, and junctions), and pipelines, which link the nodes. The model also includes water fronts as secondary agents; the motion of these through the network helps to capture the dynamic behaviour of the DHN (see Section 2.6).

The modelling of mass and energy conservation is approached as follows. The mass flow model is handled by AnyLogic’s fluid library. This employs LP to maximise mass flow through the network at discrete points in time, within the constraints imposed by valve settings and pipe flow limits. Valve settings depend on the flow requested at demand

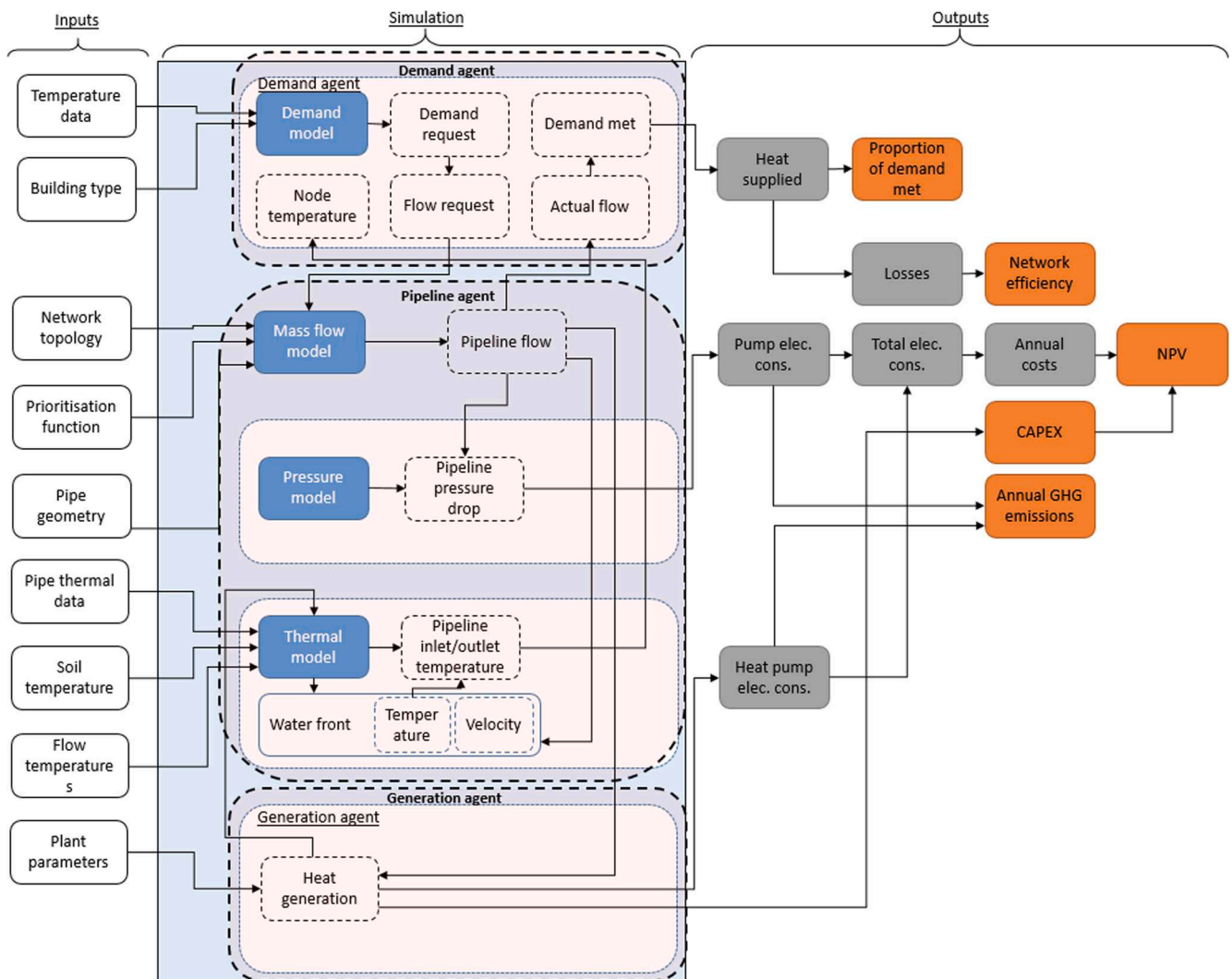


Fig. 1. An overview of the network dynamics simulation model. ‘Plant parameters’ includes locations and capacities of both boreholes and mine water sources (see Section 4).

Table 1
Definition of agents used in model.

Model Icon	Agent	Description
	Generation Centre	Industrial waste heat source, or large scale heat pump extracting heat from boreholes.
	Demand Centre	Domestic, commercial, leisure and industrial buildings with demand for space heating and hot water
	Junction	A node that allows pipe flows to split or combine.
–	Pipeline	A length of pipe that connects demand and generation centres allowing for the transfer of heat.
–	Water fronts	Volumes of water that move through the pipeline

nodes (see Section 2.4). Propagation of heat through the network occurs at finite speed; this behaviour is captured by the ‘water front’ agents. When the mass flow model alters the flowrate in a particular pipe, a water front is created which moves along the pipe at finite speed, experiencing thermal losses (see equations (14) and (15)). Fronts are also generated when changes to inlet temperature occur. On the arrival of the front at the end of the pipeline, the temperature at the outlet node is updated. Whilst this model is a simplification, it provides an improvement on equilibrium models [56]. Water pressure throughout the network is calculated as specified in Section 2.6.1, to check that the pressure remains in acceptable limits and assess the energy requirement for pumping. Pumps are located at junctions and generation centres.

The model can work with arbitrary heat sources and network scales / layouts. Here, the identification of locations for mine water or industrial heat sources is extraneous to the model: see Section 4. The specified network topology is imported to GIS, and pipe routing is decided by the model itself.

More details on the behaviour of demand agents can be found in Section 2.4; more details on the pipelines and water front agents are found in Section 2.6.

2.2. Model assumptions

To reduce the computational intensity only the phenomena that have a significant impact on the accuracy of the simulation are accounted for; therefore, the following simplifications have been made, similar to work of Duquette et al [57]:

- Water properties such as conductivity, specific heat capacity, and density are constant parameters.
- Water is considered an incompressible fluid.
- Flow within pipeline agents is one-dimensional.
- Heat loss to the surroundings is one-dimensional.
- There is no degradation of piping material or insulation over the simulation time.
- Axial conduction along pipes is considered insignificant.
- The pressure drops in the pipeline agents have negligible viscous heating effects.
- Perfect mixing and adiabatic operation are assumed when flows combine at junction agents.
- All heat is extracted from the supply and return temperature difference.
- When two flows combine, pressure is assumed to match the lowest inlet pressures to ensure no backflow.
- Pumps for pressurisation are installed at generation centres and junctions only.
- Non-constant terms in the momentum equation are neglected.
- Pressure loss within the HIU at the demand centres is not considered.
- HIU is 100 % efficient. Cooling is not considered.

The following sections provide further detail on the sub-models.

2.3. Generation centres

Generation centres are assigned a capacity P_{GC} in kW_{th}. The maximum volumetric flow of water $\dot{V}_{GC,max}$ from the generation centre is a function of C_{GC} , flow temperature for the generation (which is assumed constant) and the return temperature. It is also constrained by the radius r_{GC} of the pipeline connecting to the generation centre:

$$\dot{V}_{GC,max} = \min \left(\frac{P_{GC}}{c_w \rho_w (T_{GC,flow} - T_{GC,return})}, \pi v_{max} r_{GC}^2 \right) \quad (1)$$

where c_w and ρ_w are respectively the specific heat capacity and density of water, and v_{max} is the maximum flow velocity allowed in the pipeline. $\dot{V}_{GC,max}$ is passed to the fluid model. The actual value of \dot{V} in the interval $[0, \dot{V}_{GC,max}]$ is determined by the level of demand downstream.

2.3.1. Geothermal plants

The geothermal plants use boreholes to extract mine water energy. They are equipped with large-scale heat pumps that supply heated water to the distribution network at a defined network temperature. The sustainable annual heat extraction from the borehole is calculated as:

$$Q_{annual,max} = \frac{8760}{1000} \bullet q \bullet SA \quad (2)$$

where SA is the total surface area of the mine workings; q is the heat flux from surrounding ground to the mine water; and the factor 8760/1000 converts Watts to kWh/a. Designed annual heat extraction should be below this level, as specified in Equation (3):

$$\int_0^{8760} \dot{Q}_{borehole} \bullet dt \leq Q_{annual,max} \quad (3)$$

where $\dot{Q}_{borehole}$ is heat extraction from the borehole in kW_{th}. Heat pumps are used to increase the mine water temperature to the required flow temperature. Owing to the steady temperature of the mine workings, these are expected to have relatively constant COP in the range 3 – 6 [45]. Electrical power consumption of the heat pump P_{HP} and total heat supply \dot{Q}_{gen} are linked to $\dot{Q}_{borehole}$ via equations (4) and (5) [58].

$$\dot{Q}_{borehole} = \dot{Q}_{gen} \frac{COP - 1}{COP} \quad (4)$$

$$P_{HP} = \frac{\dot{Q}_{gen}}{COP} \quad (5)$$

2.3.2. Industrial waste heat

Industrial waste heat sources function similarly to other generation centres, but with variations in the parameter values for costs, efficiency, and maximum power generation output. Industrial waste heat refers to the unused heat produced as a by-product of various industrial processes.

2.4. Demand centres

As noted above, demand centres attempt to procure the required amount of heat $\dot{Q}_{DC,demand}$ by adjusting the flow rate of water through the valve.

$$\dot{V}_{DC,max} = \frac{1000 \bullet \dot{Q}_{DC,demand}}{c_w \rho_w (T_{DC,flow} - T_{DC,return})} \quad (6)$$

Actual supply may deviate from demand: this is because constraints on flow at generation centres and in pipelines may lead to $\dot{V}_{DC} < \dot{V}_{DC,max}$;

and also because values of T_{flow} and T_{return} may vary from their values when the control action was taken. Thus the actual instantaneous heat supplied is given by Equation (7):

$$\dot{Q}_{DC,demand} = \frac{1}{1000} c_w \rho_w \dot{V}_{DC} (T_{DC,flow} - T_{DC,return}) \quad (7)$$

Demand centres are prioritised according to their distance from the generation. If the demanded hot water flow is more than the DHN can provide, supply is prioritised for the nodes nearest to the generation. For domestic demand, each demand centre represents the aggregation of tens to hundreds of houses; for non-domestic demand, one demand centre represents one building. The model for heat demand will now be detailed.

2.4.1. Demand model

Heat demand in the simulation is modelled using piecewise linear regression against ambient temperature T_{ext} , with a different regression for each building type, each of twelve daily time intervals, and each of two seasons; similar to the approach in [59]. Building types considered are: ‘domestic’, ‘leisure’, ‘residential’, ‘commercial’ and ‘education’. (‘Residential’ refers to large demands such as hotels and blocks of flats and therefore differs from ‘domestic’.) For a given building type, demand is given by Equation (8):

$$\dot{Q}_{demand}(t, T_{ext}) = \begin{cases} (m_{t,1} T_{ext} + c_{t,1}) + e_t, \text{ for } T_{ext} \leq \hat{T}_t \\ (m_{t,2} T_{ext} + c_{t,2}) + e_t, \text{ for } T_{ext} > \hat{T}_t \end{cases} \quad (8)$$

Here t represents the timeslot within the day; $m_{t,i}$ and $c_{t,i}$ represent the coefficients for the piecewise linear model at time t ; \hat{T}_t represents the boundary temperature between the two linear sections; and e_t represents an error term. Fig. 2 illustrates heat demand (measured in kW) on the y-axis and air temperature ($^{\circ}\text{C}$) on the x-axis. Multiple lines are shown, each representing an average heat demand for specific two-hour intervals throughout a 24-hour day. For instance, there are distinct lines representing the intervals from midnight to 2 am, 2 am to 4 am, and so on for the entire day.

It will be seen that the model depends on values for the parameters $m_{t,i}$, $c_{t,i}$ and \hat{T}_t . These were regressed against measured data to obtain a least squares fit. For the ‘domestic’ category, regression was carried out against data from the renewable heat premium payment (RHPP) scheme [60]. This demand was for heat pumps, so the assumption here is that demand profiles are relatively independent of heating system. Since the model is intended to represent domestic heat demand only at the resolution of hundreds of houses, the regression used 138 houses and 134

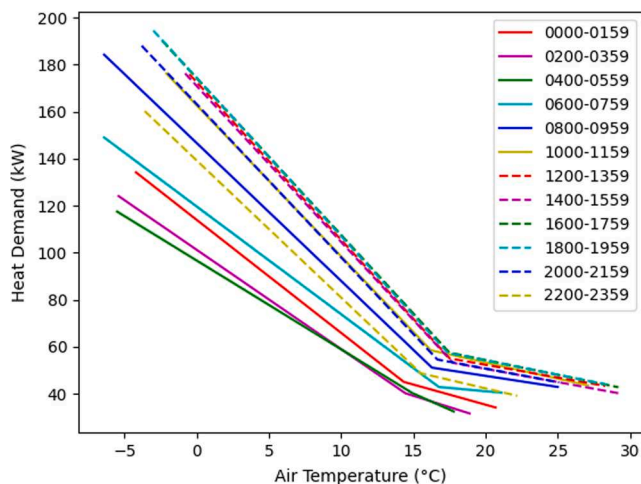


Fig. 2. Piecewise linear regression of heat demand versus ambient temperature for the ‘residential’ category.

houses respectively for the winter and summer models, as dictated by the availability of good quality data. Domestic demand centres in the simulation have demand rescaled according to the number of addresses.

For the remaining building categories, regression was carried out against hourly heat network demand data procured from a third party; this data included 47 educational, 41 commercial, 15 residential and 9 leisure buildings. For these building types, each demand centre corresponds to one building, and demand is rescaled by floor area.

The MIDAS database [61] was used for temperature data, both for model-fitting and for the final simulation. Error terms e_t reflect the variance of the measured data around the piecewise linear fit and provide the final simulation model with an element of stochasticity. The final adjustment to heat demand is to ensure that it is non-negative (cooling is not considered in the model).

This study utilised third-party data to validate the model, aligning it with real-world conditions. To establish a robust validation framework, the network model was configured to precisely correspond to the nodes of this third-party data. However, specifics of the validation are protected under a Non-Disclosure Agreement (NDA), which restricts the direct representation of raw figures.

Despite the constraints of the NDA, overall validation results affirm the model’s effectiveness and robustness. Minor temperature profile variances between the simulation and real-world data were observed. These discrepancies can largely be attributed to the simulated demand of non-domestic buildings, which had limited data available for validation.

Fig. 3 showcases the comparison between the average modelled demand and the actual demand from the third-party data for domestic buildings. The results from the domestic demand centre model indicate an average heat demand of 12.3MWh per year for each building. This closely aligns with data provided by BEIS, which estimates an average heat demand of 12MWh per household annually [62]. The alignment of these figures underscores the model’s fidelity to real-world observations, attesting to its reliability.

2.5. Junctions

Junctions allow the combination of two or more network pipes. To calculate the outlet pipe temperature under adiabatic conditions it is assumed that perfect mixing occurs instantly. The outlet temperature is

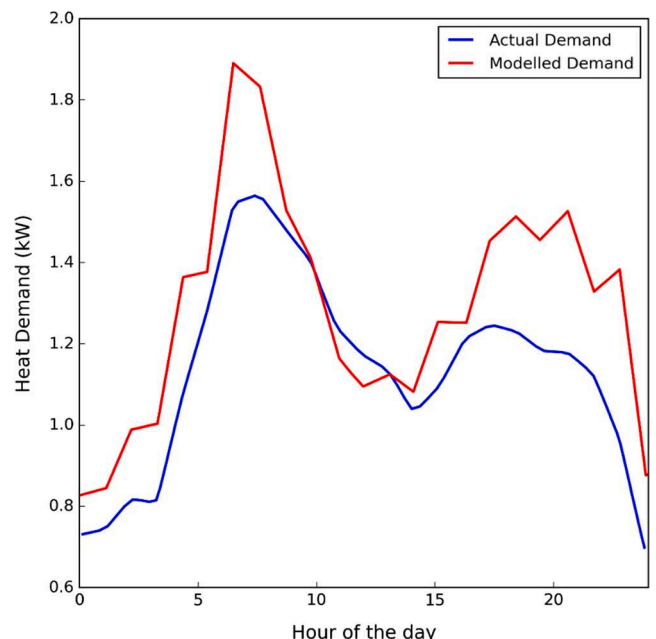


Fig. 3. Average daily profile for a single domestic building.

then a weighted average of the inflow temperatures [63]:

$$T_{junc} = \frac{\sum_i \dot{m}_i T_i}{\sum_i \dot{m}_i} \quad (9)$$

where T_{junc} is the temperature exiting the junction at time t , m_i is the mass flowrate into the junction at time t .

2.6. Pipelines

Pipelines are characterised by their route, length, diameter and the thicknesses of insulation and other layers. To adhere to vibration regulations and to decrease the friction/degradation of the pipework, each pipe is throttled to a maximum volumetric flow rate $\dot{V}_{p,max}$ [64] determined by cross-sectional area CSA_p and a maximum flow velocity v_{max} :

$$\dot{V}_{p,max} = CSA_p \cdot v_{max} \quad (10)$$

Each pipe is linked to a unique start and end node. The route between these (and resulting pipe length) is obtained using the Open Street Map server [65].

The flow rate through the pipe is determined by the fluid model, as outlined in Section 3.1. Temperature dynamics in the pipe are modelled as follows. Input and output temperatures $T_{p,in}$ and $T_{p,out}$ are defined for the pipe at all times. The pipe operates under one of two modes: FLOWING and ZERO_FLOW. Under the first mode, the outlet temperature is dictated by the arrival of 'water front' agents. Under the second mode, outlet temperature decays continuously towards soil temperature.

R' describes the thermal losses of the pipeline as Watts per meter of length per °K. It results from the combination of five thermal resistances: the interface between fluid and pipe; the pipe wall, insulation and casing; and the interface between pipe and soil. Equation (11) gives the definition [57]:

$$R' = \frac{1}{(2\pi(r_{in} \times 10^{-3})h_{co})} + \frac{\log\left(\frac{r_{pipe}}{r_{in}}\right)}{2\pi k_{AB}} + \frac{\log\left(\frac{r_{insulation}}{r_{steel}}\right)}{2\pi k_{BC}} + \frac{\log\left(\frac{r_{casing}}{r_{insulation}}\right)}{2\pi k_{CD}} + \frac{1}{(Fk_s)} \quad (11)$$

Here k_{AB} , k_{BC} , k_{CD} and k_s are the thermal conductivities respectively of the pipe wall, pipe insulation, pipe casing and soil. r_{pipe} , $r_{insulation}$ and r_{casing} give the outer radii of the pipe, the pipe insulation and pipe casing. h_{co} is the convection coefficient with unit's W/K, and F is a dimensionless shape factor.

The value of R' and all related quantities is updated whenever the fluid flow through the pipe changes.

The convection coefficient h_{co} is dependent on the fluid and flow properties and is calculated by Equation (12) [57]:

$$h_{co} = \frac{Nu \cdot \sigma_w}{2(r_{in} \times 10^{-3})} \quad (12)$$

where σ_w is conductivity of water, r_{in} is the internal radius of the pipe and Nu is Nusselt's number. Details on the calculation of Nu can be found in Appendix A.2. The shape factor F is calculated as in Equation (13) [66]:

$$F = \frac{2\pi}{\operatorname{acosh}\left(\frac{d}{r_{in} \times 10^{-3}}\right)} \quad (13)$$

where d is the burial depth of the pipe.

Change of flowrate or input temperature triggers the creation of a water front agent; this travels along the pipe with speed dictated by the water flowrate. The temperature of the water front evolves according to Equation (14):

$$c_w \cdot \rho_w \cdot A \cdot \frac{dT}{dt} = -\frac{T - T_s}{R'} \quad (14)$$

where T_s is the temperature of the surrounding soil, assumed constant. Equation (15) yields the exact solution:

$$T(t) = T_s \cdot (1 - \Lambda) + T_0 \cdot \Lambda \quad (15)$$

with $\Lambda := \exp\left(-\frac{t}{c_w \rho_w A R'}\right)$, where T_0 is equal to the value of $T_{p,in}$ at the time of water front creation, and t is time elapsed since water front creation. This is similar to models found in Duquette et al [57] and others. Upon arrival at the end of the pipeline, the destination node temperature is updated with the temperature of the arriving water front. For simplicity, in FLOWING mode this outlet temperature remains constant in between the arrival of water fronts. Thus, the model operates as an equilibrium model after a delay while water fronts are in transit.

If flow in the pipe is zero, $T_{p,out}$ is expected to decay towards T_s . In this case, the mode of the pipe is switched to ZERO_FLOW and $T_{p,out}$ evolves according to equations (14) and (15).

For the network's return pipes, the water fronts are omitted and a OD model is used. Return pipe temperature thus evolves according to Equation (16):

$$\dot{T}_{return,p}(t) = \frac{Q_{return,p}}{\rho_w \cdot c_w \cdot \pi \cdot r_{in,p}^2 \cdot L_p} \quad (16)$$

where $T_{return,p}$ is the return pipe temperature at time t , $Q_{return,p}$ is the energy transferred to the return pipe, ρ_w and c_w are the density and specific heat capacity of water, respectively, $r_{in,p}$ is the radius of the pipe, and L_p is the length of the pipe.

2.6.1. Pressure drop and pump requirements

Pressure drop ΔP occurs due to frictional losses and is dependent on the flow regime. The pressure drop is affected by the length of the pipe and the fluid velocity. Equation (17) describes this [67]:

$$\frac{\Delta P}{L_p}(t) = u \left(\frac{\dot{v}_x^2(t) \rho_w}{2r_{in}} \right) \quad (17)$$

where u is the unitless friction factor, r_{in} is the radius at the inlet of the pipe and ρ_w is the density of water. ΔP is the pressure drop in the pipe, L_p is the length of the pipe, \dot{v}_x is the volumetric flowrate at time t .

The overall pumping power requirement P_r can be expressed by Equation (18) [68]:

$$P_r = \frac{\int_0^{8760} \Delta P \cdot \dot{v}_x \cdot dt}{\eta_{pump} \cdot \eta_{motor}} \quad (18)$$

where η_{pump} and η_{motor} are the pump efficiency and electric motor efficiency, respectively.

3. Techno-economics

3.1. Emissions

Techno-economics are concerned with the cost-effectiveness and environmental impact of the heat network. The GHG emissions are computed following the UK Government's GHG Conversion Report [69]. The efficiency of the heat network is calculated by Equation (19):

$$\eta = \frac{Q_s}{Q_g} \cdot 100\% \quad (19)$$

where η is the overall efficiency of the network, Q_g is the total heat generation from geothermal plants, and Q_s is the actual heat supplied to demand centres.

The percentage of demand met is calculated by Equation (20):

$$Demand_{met} = \frac{Q_d}{Q_s} \bullet 100\% \quad (20)$$

where Q_d is the demand requested by the network.

Standalone boilers are used in the business-as-usual case, relative to which the DHN's carbon emissions are compared. Carbon emissions from boilers are calculated using a carbon factor from The Standard Assessment Procedure [70] in Table 2 that quantifies the CO₂ released per kWh of energy use. The same heat demand model is used as specified in 2.4. The emissions from boilers are calculated by Equation (21):

$$CO2_b = \frac{Q_d}{\eta} \bullet f_b \quad (21)$$

where $CO2_b$ is the carbon emission from the boilers, η is the efficiency of the boilers, and f_b is the carbon factor of the boilers.

The CO₂ emissions from the geothermal plants and industrial waste heat are calculated by Equation (22), the emissions from the heat pumps by Equation (23), and the emissions from the repressurising pumps by Equation (24), using the carbon factors from Table 2:

$$CO2_{gc} = Q_{g,gc} \bullet f_{gc} \quad (22)$$

$$CO2_{hp} = \sum_{m=1}^{12} \frac{Q_{g,m}}{COP} \bullet f_{e,m} \quad (23)$$

$$CO2_p = \sum_{m=1}^{12} E_{p,m} \bullet f_{e,m} \quad (24)$$

where $CO2_{gc}$, $CO2_{hp}$, $CO2_p$, are the carbon emissions from the geothermal plants, heat pumps and repressurising pumps, respectively, $Q_{g,gc}$ is the heat generated by a GC, $Q_{g,m}$ is the monthly heat generation from a GC, $E_{p,m}$ is the monthly emissions from the pumps, f_{gc} , $f_{e,m}$ are the carbon factor for geothermal energy plants and electricity, respectively.

The total CO₂ emissions $CO2_{total}$ from the DHN are calculated by Equation (25):

$$CO2_{total} = CO2_{gc} + CO2_{hp} + CO2_p \quad (25)$$

Equation (26) gives the percentage carbon savings $CO2_s$ relative to boilers:

$$CO2_s = \frac{CO2_b - CO2_{total}}{CO2_b} \bullet 100\% \quad (26)$$

Marginal reduction in emissions for the region is calculated by Equation (27):

$$CO2_{MR} = 100 - \frac{CO2_{bT} - CO2_b + CO2_{total}}{CO2_{bT}} \bullet 100\% \quad (27)$$

where $CO2_{bT}$ is the emission from the entire region, and $CO2_{MR}$ is the percentage marginal reduction.

3.2. Costs

The following equations are used to calculate various costs of the network and any currency specified is originally in pounds or has been converted. The network piping costs are calculated by Equation (28):

Table 2
Carbon factors [70].

Source	Carbon factor (t/MWh)
Geothermal plant	0.011
Industrial waste heat	0.011
Natural gas	0.210
Electricity (Monthly average)	0.136

$$CC_N = (C_{BP} + C_{IP}) \bullet L_T \quad (28)$$

where CC_N is the total network piping cost, C_{BP} is the main buried pipe cost factor and C_{IP} is the internal pipe cost factor and L_T is the total network length.

The demand centre cost is calculated by Equation (29):

$$CC_{DC} = (C_N + C_{SS} + C_{HM} + C_{HIU}) \bullet Q_d \quad (29)$$

where CC_{DC} is the total demand centre cost, C_{SS} is the cost factor of the substation, C_{HM} is the cost factor of heat meters, and C_{HIU} is the cost factor of the heat interface unit.

The cost of heat pump follows an affine relationship vs capacity in MW is obtained from Pieper et al [71], shown in Fig. 12, in Appendix A.3, thus calculated by Equation (30):

$$CC_{HP} = (0.6398 \bullet C + 0.50543) \quad (30)$$

where CC_{HP} is the capital cost of the HP, and C is the maximum capacity of the HP for the specific network.

The ancillary equipment cost is calculated using Equation (31):

$$CC_A = Q_d \bullet C_A \quad (31)$$

where CC_A is the capital cost of ancillary equipment and C_A is the cost factor of the ancillary equipment.

Total capital cost of the network is calculated by Equation (32):

$$CC_t = CC_N + CC_{DC} + CC_{HP} + CC_A \quad (32)$$

where CC_t is total capital cost of the network.

The O&M costs are calculated by Equation (33).

$$O\&M = C_B \bullet C + (C_{NM} + C_{HIUM} + C_{HMM} + C_{SC} + C_{BR})Q_g + P_{HP} \bullet E \quad (33)$$

where O&M represents the total operation and maintenance costs, C_B is the operational cost factor of a borehole, C_{NM} , C_{HIUM} , C_{HM} , C_{SC} , C_{BR} is the operational cost factor for network maintenance, HIU maintenance, heat meter maintenance, staff costs and business rates, respectively. P_{HP} is the electrical power consumption of the heat pump and E being the price of electricity.

Energy cost is calculated by Equation (34):

$$E_t = \frac{Q_g}{COP} \bullet E \quad (34)$$

where E_t is the total energy cost.

Inflation is taken into account; thus, the real discount rate can be calculated from the nominal discount rate and inflation rate using Equation (35) [72]:

$$R = \frac{(1 + R_{nom})}{(1 + i)} - 1 \quad (35)$$

where r is the real discount rate, r_{nom} is the nominal discount rate and i is the inflation rate.

Net-present cost (NPC) is a metric to assess the costs of a heat network considering monetary outflows over time. For networks without industrial waste heat and with industrial waste heat the NPC is calculated using Equation (36) and (37), respectively [73], incorporating total capital, operational and energy costs. The model will be integrated into the electricity grid to realise profits and a positive NPV obtained in future work.

$$NPC_a = \sum_{t=0}^n \frac{CC_t + O\&M + E_t}{(1 + R)^t} \quad (36)$$

$$NPC_b = \sum_{t=0}^n \frac{CC_t + O\&M + E_t + (Q_{WH} \bullet C_{WH})}{(1 + R)^t} \quad (37)$$

where subscripts b and a denote with and without industrial waste heat respectively, and Q_{WH} is the industrial waste heat energy usage and C_{WH} its cost factor.

The Levelized Cost of Heat (LCOH) is a metric to assess the cost heat delivery to the network over its lifetime and is calculated without industrial waste heat and with by Equation (38) and (39), respectively. It depends on the heat generation and demand requested, length of pipe-work, substations, and plants contributing to capital and operational costs [74].

$$LCOH_a = \frac{\sum_{i=1}^n (CC_i + O\&M_i + E_i) / (1 + R)^i}{\sum_{i=1}^n Q_i / (1 + R)^i} \quad (38)$$

$$LCOH_b = \frac{\sum_{i=1}^n (CC_i + O\&M_i + E_i + (Q_{WH} \cdot C_{WH})) / (1 + R)^i}{\sum_{i=1}^n Q_i / (1 + R)^i} \quad (39)$$

where subscripts b and a denote with and without industrial waste heat respectively, LCOH is the levelised cost of heat achieved by the network and Q_i is the total energy.

4. Case study

The model detailed in sections 2 and 3 is employed to assess the feasibility of a mine water district heat network in Barnsley. The local council of Barnsley has envisioned four distinct network layouts, each leveraging the latent thermal energy of the surrounding mine workings. This represents the evolution of a district heat network temporally. These networks share a constant baseload of non-domestic connections, but exhibit variations in the extension of domestic connections, thus affecting network lengths and heat densities. All networks have a consistent number of geothermal plants, but variants include an additional pipe from a glass manufacturer supplying waste heat, augmenting the network length and generation capacity.

Performance evaluations were based on a year-long simulation using 2021 temperature data [75], with supply and return temperatures set at 60 °C and 30 °C respectively but will vary depending on performance of the network. The network piping is assumed to be at a burial depth of 0.8 m with a soil temperature of 10 °C [76].

Firstly, the potential sites for initial geothermal plants were identified, revealing four mine-working locations and four boreholes with adequate ambient temperatures. Further data on the boreholes intersecting these workings are presented in Table 3 obtained from old mine workings maps supplied by The Coal Authority [77]. A heat flux q value of 63.5 Wm^{-2} was used [44].

4.1. Network classification

The selection and classification of demand is found in Appendix A.1. The baseline COP is assumed to be 4.9 [78]. The areas in close proximity to the boreholes contain 12,636 buildings, with each demand centre node containing between 65 and 375 domestic houses. A mixture of 25 non-domestic buildings (5 commercial, 11 education, 2 leisure, 7 residential) identified will be used as anchor loads. Table 4 shows each borehole and the number of nearby non-domestic and domestic buildings.

Four scenarios are outlined in Table 5, each with an increasing number of domestic demand centers attached; this is designed to scale

Table 3
Borehole depth and temperature.

Borehole	Depth (m)	Temperature (°C)	Surface Area (m^2) $\times 10^6$
Grimethorpe	150	14.3	90.1
Houghton	243	14.9	64.3
Royston	332	17.9	84.3
Cudworth	132	18.2	34.3

Table 4

Number of DC of each building classification and the total number of buildings.

Village	Building Type	No. of DCs	No. of Buildings
Grimethorpe	Domestic	21	5650
	Non-domestic	16	–
Houghton	Domestic	15	3549
	Non-domestic	8	–
Royston	Domestic	13	3437
	Non-domestic	1	–

the network.

Network parameters and costs [79] are outlined in Table 6 and 7 with carbon cost taken from UK ETS [80] discount and inflation rate from The Green Book [81] and COP from Fig. 13, in Appendix A.4 estimated from the supply and return temperature values. Where p is used in p/kWh this refers to pennies (£0.01) per kWh of heat delivered.

4.2. Pipe sizing

To determine the appropriate pipe size for the DHN's a heuristic approach and Insulation Class 1 selection criterion [82] are used. The nominal pipe diameters are initially calculated based on the velocities prescribed by the UK Heat Network Code of Practice [83], as illustrated in Fig. 14 in Appendix A.5. Subsequently, trial simulations were conducted, and various performance indicators were recorded, including velocity, demand supply deficit, and network efficiency. The position of the pipe in the network and the number of downstream connections were also considered. In case any pipe was throttled due to the maximum velocity, it was adjusted to the next size, and similarly for undersized pipes. It is worth noting that pipe sizes remained unchanged for all scenarios.

4.3. Industrial waste heat

In addition to the network's mine water heat supply, an additional source of heat can be obtained from a nearby glass manufacturer, with a maximum capacity of 7 MW obtained through conversation with Barnsley region council [84], which can be utilised at any given time. This industrial waste heat resource presents an opportunity to supplement the overall heat generation. It operates with an efficiency of 90 % [85] and adds an additional 1.11 km of pipework to each network scenario.

The cost associated with utilising the industrial waste heat is 3 pence per kilowatt-hour (p/kWh) [86]. This cost reflects the price charged for accessing and utilising the industrial waste heat output. It is important to note that the industrial waste heat option provides a cost-effective means of obtaining heat, considering its comparatively lower cost per unit of energy compared to other sources.

The chosen case study serves as an exemplary scenario for strategic investment in mine water heat networks, particularly due to Barnsley's proximity to geothermal heat sources and disused coal mines. This model has been designed specifically to evaluate diverse demand scenarios and scale of network, thereby assessing the feasibility of the region for decarbonisation and its potential for transformation. The assessment of cost-effectiveness in reducing CO₂ emissions from stand-alone boilers would provide valuable insight, with the ambition of informing the district about the possible innovation avenues within its heating sector.

5. Results

This section presents the results of applying the methods discussed in Section X, thereby developing DHNs that employ both mine water energy and industrial waste heat. Four network scenarios (S1-S4) of increasing complexity were evaluated, each represented by two variants

Table 5
Number of buildings in each scenario.

Scenario	1	2	3	4
Number of buildings	3184	6343	9502	12,661
 = 1000 buildings				
Network Length (m)	37,512	42,581	45,451	52,775

Table 6
Network parameters.

	Value
Pump efficiency (%)	80
Motor efficiency (%)	80
Network pressure (kPa)	1,500
Supply temperature (°C)	60
Return temperature (°C)	30
Soil temperature (°C)	10
Water conductivity (W/mK)	0.598
Water diffusivity (mm ² /s)	0.16
Lifetime (years)	30
COP	4.9

Table 7
Cost parameters.

	Value
Electricity price (p/kWh)	13
Gas price (p/kWh)	4.94
Combined operation costs (£/kWh)	35.9
Combined demand Centre costs (£/kWh)	919
Substation cost (£/kWh)	16
Ancillary cost (£/kWh)	68
Combined pipework cost (£/kWh)	516
Boiler CAPEX and OPEX cost (£/kWh)	2.28
Inflation rate (%)	2.7
Discount rate (%)	3.5
Carbon cost (£/MWh)	52.56

- one with and one without industrial waste heat. The techno-economic aspects and environmental benefits are both assessed.

5.1. Network performance

Fig. 4 provides a heat plot illustrating the dynamic daily heat demand patterns throughout the year, captured by the network. The time of day is plotted on the y-axis and days of the year on the x-axis, the plot corroborates the following well-established trends in DHN usage: firstly, an observable surge in heat demand during the morning hours, likely attributable to space heating needs after a cold night and hot water usage for daily routines (a). Secondly, a pronounced peak in heat

demand during late afternoon and early evening hours, reflecting the increased usage of heat for activities such as cooking, bathing, or space heating (b). Finally, an appreciable reduction in heat demand during summer months, attributed to warmer outdoor temperatures and consequent decreased reliance on the DHN for space heating (c). The average household heat demand per year was calculated at Table 8 outlines the key performance indicators of different network scenarios both with and without the incorporation of industrial waste heat. The parameters evaluated in these scenarios include heat generation (MWh), heat demand (MWh), heat supply (MWh), the percentage of demand met, emission savings (%), carbon factor (kgCO₂/MWh) and pump power (MWh). The table shows the variations in these parameters as the network size increases from S1 to S4.

For networks without industrial heat, heat generation and heat

Table 8
Key performance indicators of scenarios.

Network (w/o industrial waste heat)	Unit	S1	S2	S3	S4
Heat generation	MWh	111,000	148,600	168,600	214,200
Heat demand	MWh	97,100	131,300	150,100	197,200
Heat supply	MWh	96,400	129,200	147,100	173,400
Demand met	%	99.2	98.4	98.0	87.9
Emission savings*	%	80.57	80.60	80.68	80.83
Carbon factor	kgCO ₂ eq/MWh	50.50	49.58	48.95	41.43
Pump power	MWh	1620	3550	4980	7370
Network (w/ industrial waste heat)	Unit	S1	S2	S3	S4
Heat generation	MWh	106,600	149,400	170,700	204,700
Heat demand	MWh	96,300	130,000	149,000	198,800
Heat supply	MWh	90,500	127,900	146,800	178,000
industrial waste heat usage	MWh	31,200	37,300	40,400	40,500
Demand met	%	94.0	98.6	98.3	89.5
Pump power	MWh	1950	4040	5110	7270
Emission savings*	%	85.02	84.48	84.35	83.88
Carbon factor	kgCO ₂ eq/MWh	36.55	39.25	39.55	35.75
Change in LCOH	%	8.36	6.71	6.22	5.56

* Using the same demand of that specific network but consisting of boilers only.

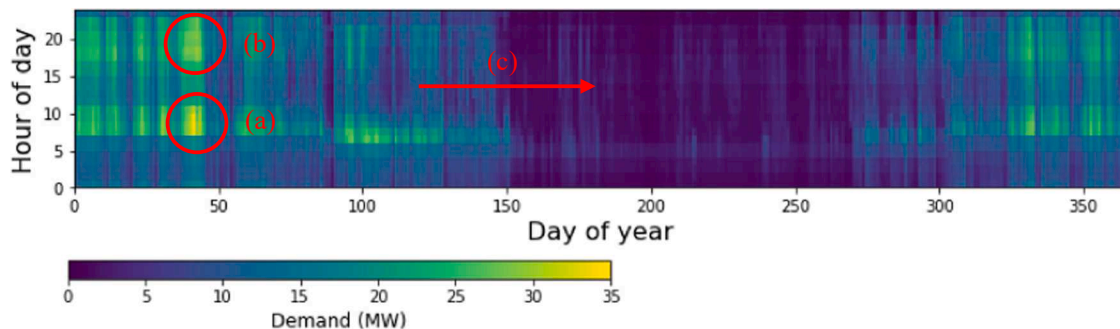


Fig. 4. Heat plot of demand across the network for S1.

demand increase with growing network size, S1 through S4. The demand met, however, declines as the network size increases, with a decrease from 99.2 % in S1 to 87.9 % in S4. Emission savings display an upward trend across the scenarios, indicating a higher emission reduction as the network size grows. Notably, the carbon factor decreases with the network expansion. Pump power, indicative of the energy used by the pump, escalates with increasing network size.

In scenarios incorporating industrial heat (S1WI-S4WI), the heat generation, heat demand, and industrial heat usage all increase with the network's size. However, the percentage of demand met decreases. This trend is also observed in scenarios without industrial heat. The carbon factor increased from S1WI to S2WI by 7.4 %, meanwhile from S3WI to S4WI there was a decrease by 9.6 % indicating a mixed trend. Changes in LCOH from S1WI to S4WI decreased across the scenarios from, with a difference of 2.8 %. Understanding these nuances allows us to better navigate the complexities and potential challenges in designing and expanding heat networks, especially when incorporating industrial heat.

Fig. 5 represents the correlation between heat loss and efficiency all network scenarios, with and without the incorporation of industrial waste heat. It demonstrates a clear trend of increasing efficiency and decreasing heat loss as the network size expands, for both scenarios with and without industrial waste heat. This trend is indicative of the advantages of larger networks in enhancing operational efficiency and managing heat loss. However, an intriguing observation is that networks utilising industrial heat, despite following the same trend, consistently show lower efficiency than their counterparts without industrial waste heat. This drop in efficiency is attributed to the comparatively higher thermal losses observed when industrial waste heat is incorporated into the networks due to the higher supply temperature and additional pipe length. This discrepancy suggests that while the integration of industrial waste heat can aid in meeting the increased demand of larger networks, it may simultaneously incur a penalty in efficiency.

5.2. Net present cost

Fig. 6 shows the comparison of NPC for all scenarios. The costs are detailed in several categories, including main network, demand centre, HP, substation, O&M, fuel, and carbon costs. As expected, as the network size increases from S1 to S4 the costs across all parameters generally exhibit an upward trend. This can be attributed to the larger infrastructure requirements and increased energy demand associated with larger networks. Notably, the fuel costs demonstrate the most substantial increase, reflecting the greater energy consumption and corresponding fuel expenditure.

The addition of industrial waste heat, however, shows a noticeable reduction in fuel costs across all scenarios. For instance, fuel costs reduce from S1 to S1WI see a reduction of 30.2 % saving £21.6 million, and similarly for other scenarios, although the reduction is less significant as the network scale increases. This cost reduction can be attributed to the more efficient utilisation of waste heat, reducing the reliance on the HP and thus electricity consumption. Similarly, the carbon costs decrease with the injection of industrial waste heat seeing an average reduction of 20.3 %.

The total NPC for scenarios incorporating industrial waste heat exhibits a consistent reduction, emphasising the economic advantage of waste heat recovery, seeing a reduction of 12.6 %, 6.8 %, 5.6 % and 2.48 % reduction from S1-S4 to S1WI-S4WI, respectively. In the boiler-only scenario, substantial fuel and carbon costs are noted. These high costs, in comparison to other scenarios, underline the energy inefficiency and environmental impact associated with natural gas, and the high COP of the HPs really show the decreased fuel consumption and cost.

5.3. Levelized cost and emissions

Fig. 7 displays the LCOH for the network scenarios, with and without the incorporation of industrial waste heat as well as standard deviation and mean error due to multiple instances of simulations run for each scenario. When industrial waste heat is not included, the LCOH values exhibit a narrow range, with minimal fluctuations observed across the scenarios. The LCOH slightly decreases from S1 to S3, and peaks in S4, indicating that the cost of heat does not consistently increase or decrease with the scale of the network. This trend suggests that factors other than network size may influence the LCOH.

Contrastingly, when industrial waste heat is integrated, an evident upward trend in LCOH with increasing network size is observed. This is because the proportion of heat from the heat pump at a higher cost must increase as the industrial waste heat has a fixed capacity. Therefore, as the network size increases the LCOH will converge towards the networks with industrial waste heat price.

However, despite this upward trend, the LCOH values with waste heat inclusion are consistently lower than its industrial waste counterparts, despite the larger network scale requiring more extensive pipework. The additional pipework costs are offset by the capital cost reductions of the heat pumps (HP), which further exemplifies the economic efficiency of waste heat utilisation.

In the integration of industrial waste heat, it was observed that the impact on LCOH lessened as the network size increased. Specifically, S1 showcased the highest LCOH reduction of 8.36 %, while S4 presented

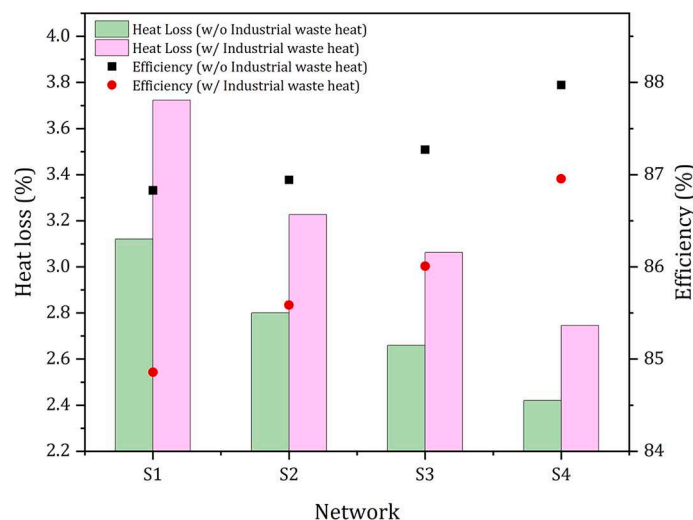


Fig. 5. Heat loss and overall network efficiency for all scenarios.

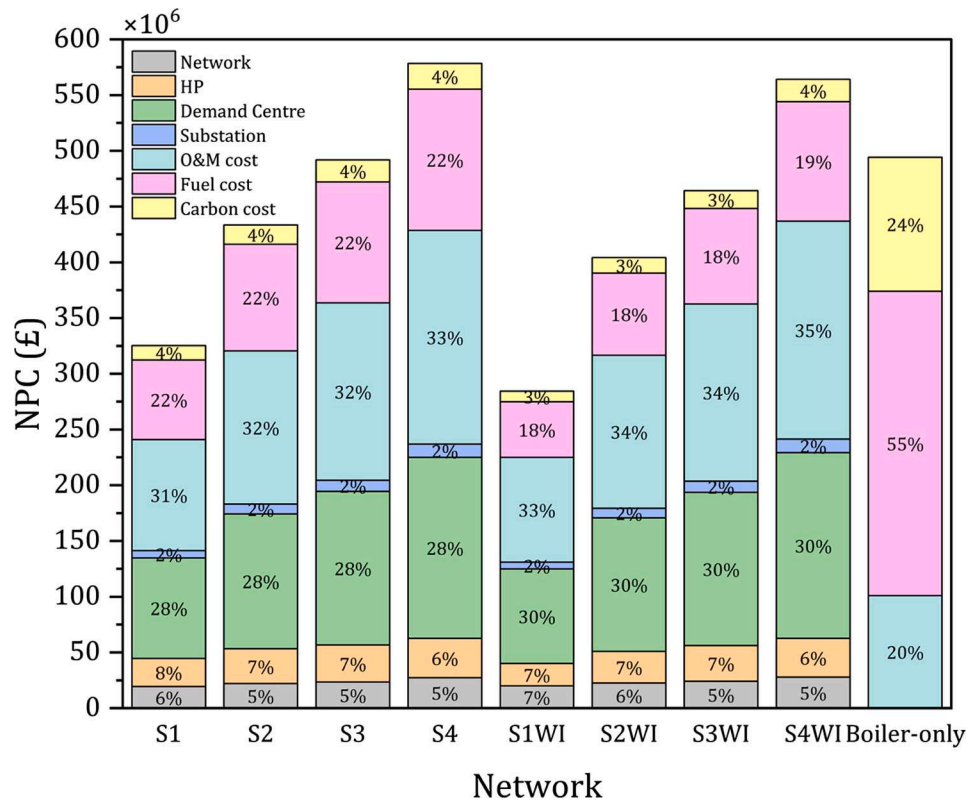


Fig. 6. Breakdown of Network Present Costs (NPC) for all scenarios, including main network, demand centre, heat pump (HP), substation, operation, and maintenance (O&M), fuel, and carbon costs.

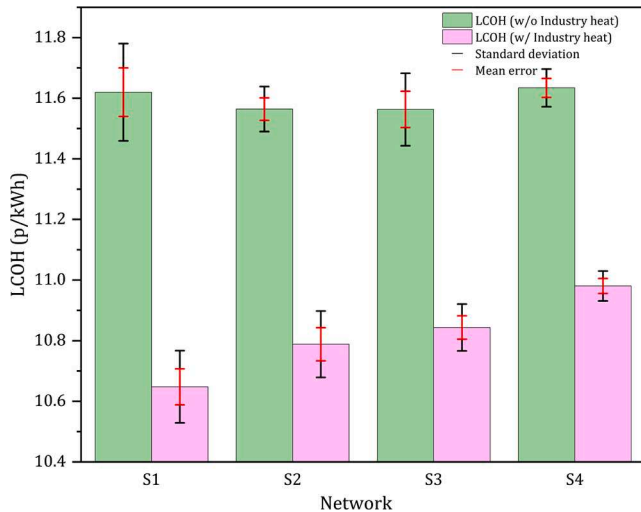


Fig. 7. Levelized cost of heat for all scenarios.

the smallest reduction of 5.62 %. This outcome suggests that waste heat’s influence on LCOH is more notable in smaller networks, where the waste heat proportion is relatively larger. Conversely, in larger networks, the waste heat proportion is smaller, thus having a smaller impact on the overall LCOH.

Fig. 8 presents the LCOH and the marginal emission reductions over all network scenarios, both without and with the integration of industrial waste heat. Marginal emission reduction, in this context, refers to the percentage decrease in CO₂ emissions achieved by each DHN scenario compared to the standalone boiler emissions of the region that isn’t connected to the DHN. This calculation effectively quantifies the emissions reduction benefit provided by each scenario.

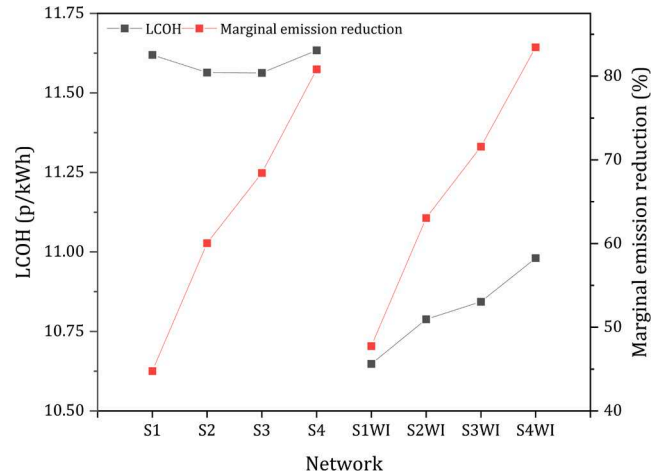


Fig. 8. LCOH and marginal reduction in emissions for scenarios.

Marginal emission reductions exhibit a significant upward trend from 44.76 % to 80.83 % for S1 to S4, respectively. Consequently, leading to greater emission reductions, despite the cost of heat remaining relatively constant.

When industrial waste heat is incorporated, the marginal emission reductions continue their upward trend but now from 47.74 % to 83.46 % for S1-S4, respectively and see a reduced LCOH from 11.62p/kWh to 10.65p/kWh for S1-S1WI. This result exemplifies the combined economic and environmental benefits of integrating waste heat into the network, yielding lower costs and higher emission reductions.

In Scenario S1, the LCOH decreases by approximately 8.36 %, while the marginal emission reduction increases by approximately 6.65 %. This shows that the inclusion of industrial waste heat in S1 brings about

a more significant economic benefit (as shown by the greater reduction in LCOH) compared to the environmental benefit (smaller increase in marginal emission reduction). Conversely, in Scenario S4, the LCOH decreases by approximately 5.62 %, while the marginal emission reduction increases by approximately 3.27 %. This indicates that while the inclusion of industrial waste heat still results in economic and environmental benefits, the relative improvements are less compared to S1. From this comparison, it's clear that the smaller network (S1) derives a greater relative economic advantage from the inclusion of industrial waste heat, while the larger network (S4) experiences a more balanced improvement between economic efficiency and environmental impact. However, the absolute environmental impact (in terms of marginal emission reduction) is higher in S4 due to its larger size and thus larger potential for emission reduction.

Of all the scenarios, the implementation of S4 with industrial waste heat presents a promising balance between cost-efficiency and environmental impact. It achieves the highest marginal emission reduction of 83.5 %, equating to a total of 38,000 tCO₂e offset, and concurrently exhibits a significant reduction in LCOH to 10.98p/kWh. The implementation of S4 thereby covers 89.5 % of Grimethorpe, Houghton, and Royston's heat demand while only producing 7,530 tCO₂e. It is notable that the adoption of S4 could contribute to a significant 21.4 % reduction in CO₂ emissions across the entire Barnsley metropolitan district [87].

5.4. Sensitivity analysis

Fig. 9 presents a sensitivity analysis of the capital costs, O&M costs, and demand for Scenarios S1 and S1WI. Specifically, the results demonstrate that a 50 % reduction in total heat demand leads to an increase in LCOH by approximately 17 % for networks without waste heat, and 13 % for networks with additional industrial waste heat. Conversely, a 50 % increase in total heat demand results in a decrease in LCOH by 5 % without industrial waste heat, and 3.5 % with industrial waste heat.

Additionally, the analysis reveals that when capital costs and O&M costs increase or decrease by 50 %, the overall LCOH follows suit, with a corresponding change of 22 % and 17 % for networks without industrial waste heat, and similar results for networks with industrial waste heat, respectively.

Furthermore, the sensitivity analysis of the LCOH for networks with industrial waste heat indicates that incorporating waste heat from industries can help reduce the sensitivity of the LCOH to changes in heat demand. This finding implies that the integration of industrial waste heat as an energy source can enhance the resilience of the DHN, making it more stable and adaptable to variations in heat demand, and

facilitating expansions or improvements in building insulation.

Fig. 10 shows the LCOH in relation to varying gas prices and COP of the HP. The figure shows the intersection S1 and S1WI. This intersection point represents the gas price at which the DHN becomes economically viable compared to boilers. Networks with industrial waste heat become competitive with boilers at a gas price of 8.7 p/kWh, whereas networks without industrial waste heat become competitive at a slightly higher price of 9.8 p/kWh. It is worth noting that natural gas prices have exhibited significant fluctuations ranging from 4.4 to 27.3p/kWh in 2021 [88]. Despite this volatility, district heating networks provide a stable LCOH.

5.5. Comparison of heating systems

Fig. 11 shows the LCOH, articulated in pence per kilowatt-hour (p/kWh), for a diverse set of heating systems. These systems span a conventional boiler, an air-to-air heat pump (HP), an air-to-water HP, a traditional CHP heat network, a DHN without industrial waste heat, and a DHN integrated with industrial waste heat.

While traditional boiler systems boast the most economical LCOH at

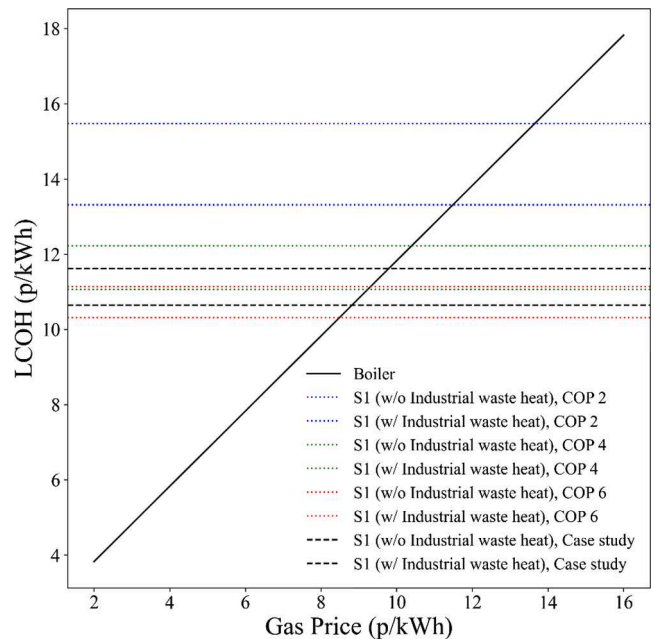


Fig. 10. LCOH of network or boilers when changing COP or gas prices.

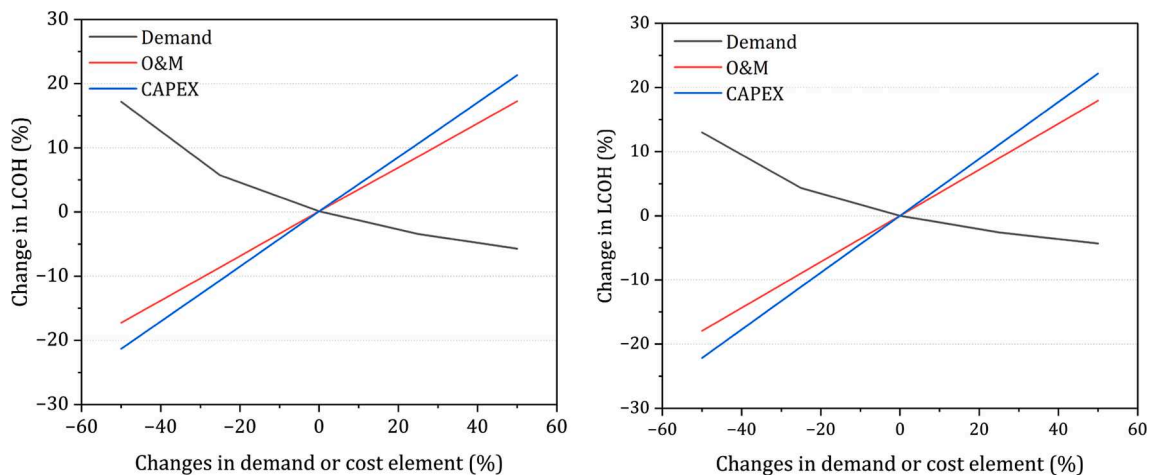


Fig. 9. Sensitivity analysis of capital, O&M costs, and demand for scenario S1 without (left) and S1WI with (right) industrial waste heat.

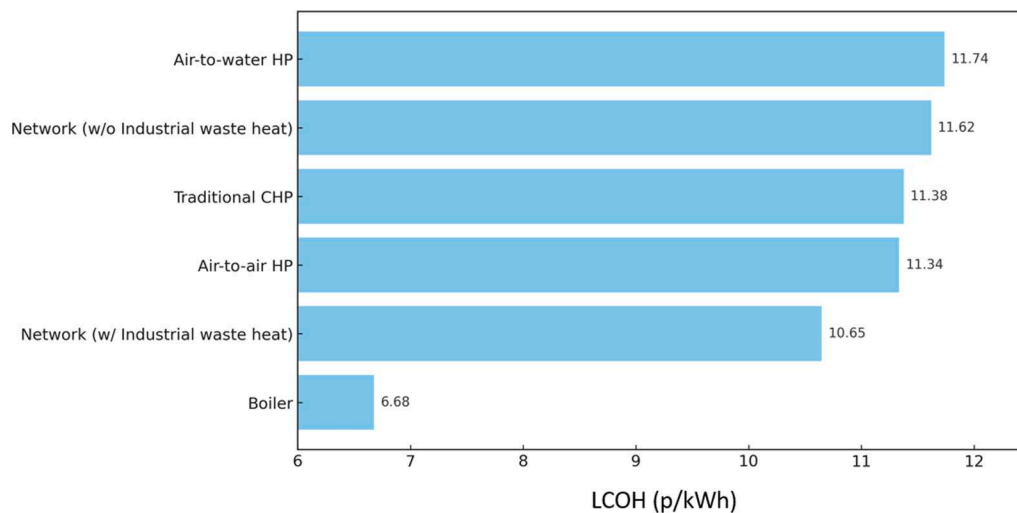


Fig. 11. Comparison of various heating systems and S4 [89].

6.68 p/kWh, their environmental repercussions are significant. Transitioning to renewables, both the air-to-air and air-to-water heat pumps log LCOH values of 11.34 p/kWh and 11.74 p/kWh respectively. Notably, the traditional CHP heat network stands at 11.38 p/kWh, positioning itself competitively within the renewable technologies.

However, DHNs, as seen, shows environmental benefits with cost efficiency. Specifically, the mine water network with industrial waste heat registers an LCOH of 10.65 p/kWh, underscoring its economic promise and better performance compared to other renewable sources.

6. Discussion & conclusion

6.1. Discussion

This research has highlighted the relationship between network size and DHN efficiency, with larger networks outperforming smaller ones, primarily due to reduced transient heat loss. Meanwhile, integrating industrial waste heat into the network offers substantial benefits but with trade-offs, moderately reducing overall efficiency due to increased thermal losses and additional piping. However, it significantly enhances the network's capacity to meet heat demand. This increased capacity is beneficial enough to outweigh the minor loss in efficiency. The assumption that "heat loss to the surroundings is one-dimensional" simplifies our understanding of these thermal losses. This foundational perspective on how these losses impact overall system efficiency influences the results, potentially underestimating multi-dimensional heat loss effects.

The value of waste heat extends beyond improved performance; it also helps make DHNs more cost-effective by reducing LCOH values. This cost-efficiency trade-off highlights the importance of waste heat as a key resource. It's important to consider the differing impacts of network size and waste heat integration on DHN system efficiency during design.

A comprehensive DHN model should factor in potential fluctuations in heat demand and cost, refining our understanding and optimisation of DHN efficiency, performance, and cost-effectiveness. The analysis of DHNs also requires understanding the interplay between economic and environmental factors. As networks expand, the balance between cost and emissions reduction becomes paramount. Larger networks, while more efficient, can incur higher operating costs, especially when integrating waste heat. Yet, they offer a significant advantage: greater reduction in emissions.

Certain scenarios, such as S1WI and S4WI, stand out due to their low LCOH and high emissions reduction capabilities. In fact, Scenario S4, when implemented with industrial waste heat, can substantially

contribute to regional decarbonisation goals. DHNs also enhance energy security and sustainability, offering stable LCOH despite natural gas price fluctuations, thus reducing reliance on fossil fuels.

The viability of large-scale networks depends on location, with regions like Barnsley well-positioned for geothermal mine water heating. Despite some demand not being met, particularly in larger networks, boreholes didn't exceed their heat extraction limits. The average household energy consumption aligns with the demand model results, indicating accuracy.

Predicting non-domestic heat demand profiles is challenging due to factors like business type, activities, opening hours, staff numbers, and building characteristics. More accurate profiles could be obtained with more building categories, but this increases complexity and may impact computational time. Supply temperature changes and pipe sizing optimisation can ensure that all heat demand is supplied and will be present in future work.

Sensitivity analysis reveals that heat demand fluctuations impact LCOH more than cost changes. Anticipated shifts in demand patterns due to factors like climate change, population growth, and changing energy usage habits are thus crucial for long-term DHN management. On the other hand, integrating waste heat can reduce the impact of demand fluctuations on LCOH, making DHNs more adaptable and stable.

Alternative heating solutions, such as ASHPs, compete with DHNs. ASHPs offer high energy efficiency but suffer performance losses in colder periods due to varying efficiency with ambient temperature. In contrast, DHNs maintain stable efficiency by using waste heat and can offer more reliable heat delivery with advanced storage technologies. Future work will look more closely at the comparison between DHN and ASHPs.

6.2. Conclusion

In the presented research, an in-depth analysis of District Heating Networks (DHNs) was executed, focusing on the integration of non-traditional heat sources, specifically mine water and industrial waste heat. Utilising a refined network dynamics simulation model with water front functionality, the investigation for Barnsley, UK yielded the following key results:

- With the expansion of the network, a clear trend in heat generation, demand, and supply emerged. Without industrial waste heat, demand satisfaction decreased from 99.2 % in Scenario S1 to 87.9 % in Scenario S4.
- The integration of industrial waste heat resulted in a 7.5 % reduction in the carbon factor by Scenario S4WI. Additionally, a transition

from Scenario S1 to S1WI led to a 30.2 % decrease in fuel costs, equating to savings of £21.6 million.

- The Net Present Costs (NPC) for Scenario S1WI was determined to be £284.46 million, indicating an advantage over the £325.36 million of Scenario S1.
- A significant 5.56 % reduction in the Levelized Cost of Heat (LCOH) was observed by Scenario S4. In comparison to traditional boiler systems, which have an LCOH of 6.68p/kWh, the traditional CHP DHN, at 11.38p/kWh, showcased competitive potential. More notably, upon the integration of waste heat, the LCOH for the network was further reduced to 10.65p/kWh, reinforcing its economic and environmental appeal.
- Despite the complexities associated with integrating multiple heat sources, Scenario S4WI maintained a thermal efficiency of approximately 87 %, even accounting for increased thermal losses.
- A critical techno-economic breakpoint was identified at a gas price of 8.7p/kWh, emphasizing the conditions under which DHNs, utilizing mine water and industrial waste heat, can economically compete with traditional boilers.
- From an environmental standpoint, Scenario S4WI achieved a marginal emission reduction of 83.5 %, showcasing the potential of the proposed DHN systems to significantly reduce regional carbon

emissions, especially in areas characterized by low heat density and outdated infrastructure.

In summary, this research offers technical insights into the viability of low-carbon DHNs in the UK, with particular relevance to regions with a rich mining history such as Barnsley. As the UK progresses towards its 2050 net-zero GHG emission targets, the findings from this study provide a valuable reference for local authorities and policy makers. For future work it is recommended to perform sensitivity analysis or optimisation of the additional pipe length and waste heat temperature to achieve peak thermal efficiency and reduce heat loss, additionally to undertake a more detailed comparative analysis with alternative heating systems.

Declaration of Competing Interest

The authors declare that they have no known competing financial interests or personal relationships that could have appeared to influence the work reported in this paper.

Data availability

The data that has been used is confidential.

Appendix

A.1. Selection and classification of demand

The following method was used within each of the three locations:

1. The postcodes within a selected village were identified using PostcodebyAddress [90].
2. The total number of properties within the village was identified by searching the EPC database for the identified postcodes[91]. An assumption was made that all the houses within each postcode had either been sold, rented, or had an EPC conducted since 2008 when the database began.
3. The villages were split into smaller postcode segments to aggregate the houses into reduced village sectors to enhance spatial accuracy. The sectors vary in size depending on the number of postcodes aggregated to obtain 200–300 houses per DC.
4. The process was repeated for each of the villages independently.

The following method was used to identify the any commercial demands within the specified region:

1. The EPC database [119] was searched for identified postcodes regions S72, S71 [91]. Both DEC and NON-DEC were obtained from the EPC database. Commercial buildings are required to have an EPC; therefore, all commercial buildings are assumed to be within the database.
2. The postcode sectors which were identified as not surrounding the 8 selected villages were removed.
3. The following categories were removed from the category type within the EPC database: a. Pubs b. Pharmacies, surgeries, and clinics. c. Retail – due to them mostly being local corner shops. d. Workshop businesses. e. Warehouse and General Industry. 4) The removal of duplicate building reference numbers and addresses was completed to eliminate any duplication.

A.2. Calculation of Nusselt's number

Reynolds number is calculated to show which regime the flow of water in the pipe, described by Equation (40):

$$Re = (4\dot{m}) \left(\pi (d_m^* 1 \times 10^{-3}) (\nu^* 1 \times 10^{-6}) \rho_w \right)^{-1} \quad (40)$$

where \dot{m} is the mass flowrate, Re is Reynolds number, d_m is the diameter of the pipe, ν is the kinematic viscosity, and ρ_w is the density of water.

Relative roughness is the amount of surface roughness that exists within the pipe and calculated by dividing the absolute roughness by the diameter of the pipe. The absolute roughness is pre-determined when sizing the pipes. Equation (41) describes this:

$$\varepsilon_R = \varepsilon_A d_m^{-1} \quad (41)$$

where $\varepsilon_{relative}$ is the relative roughness, $\varepsilon_{Absolute}$ is the absolute roughness and d_m is the diameter of the inlet pipework.

The friction factor is calculated by the Darcy-Welsbach Equation [92] and is used for calculating the friction loss in a pipe, the value is calculated by two methods dependent on the flow regime. Laminar flow is described by Equation (42):

$$\mu = 64Re^{-1} \quad (42)$$

where μ is the friction factor, and Re is Reynolds number.

Turbulent flow is described by Equation (43):

$$\mu = \left(\frac{1}{-1.8 \log_{10} 6.9 * Re^{-1} + \left(\frac{\epsilon_{relative}}{3.7} \right)^{1.11}} \right)^2 \tag{43}$$

where μ is the friction factor, and Re is Reynolds number, and $\epsilon_{relative}$ is the relative roughness.

The Prandtl Number (Pr) approximates the ratio of momentum diffusivity and thermal diffusivity, it is described by Equation (44) [93]:

$$Pr = \nu \bullet \alpha_{diff}^{-1} \tag{44}$$

where α_{diff} is the water's diffusivity coefficient.

Nusselt's Number is the ratio of convective to conductive heat transfer across a boundary surface, this is because when a fluid is motionless is conduction and convection if it involves motion. The heat flux for conduction is calculated by Fourier's law of conduction, while for convective it is calculated using Newton's Law. The ratio of these two laws gives the Nusselt's number, due to the different flow regimes the calculations are calculated differently as outlined below [94]. For laminar flow ($Re \leq 2,300$) Nusselt's number is calculated by Equation (45) (27):

$$Nu = 3.66 + \left(\frac{0.0668 Re Pr (2r_{in} (L_{route}^{-1}))}{1 + 0.04 (Re Pr (2r_{in} (L_{route}^{-1}))^{\frac{2}{3}})} \right) \tag{45}$$

where r_{in} is the radius of the pipe, L_{route} the length and Nu is Nusselt's number, Pr is Prantl's number, and Re is Reynolds number.

While, for the turbulent regime it is calculated by Equation (46), within the model this equation is used for the case of $Re > 2,300$.

$$Nu = 3.66 + \left(\frac{\mu 8^{-1} (Re - 1000) Pr}{1 + 12.7 (\mu 8^{-1})^{0.5} (Pr^{\frac{2}{3}} - 1)} \right) \tag{46}$$

where Nu is Nusselt's number, μ is the friction factor, and Re is Reynolds number, and Pr is Prantl's number.

A.3. Total Heat Pump Investment

Fig. 12 shows how heat pump capacity (MW) varies with total investment (million Euro) used in the techno-economic calculations.

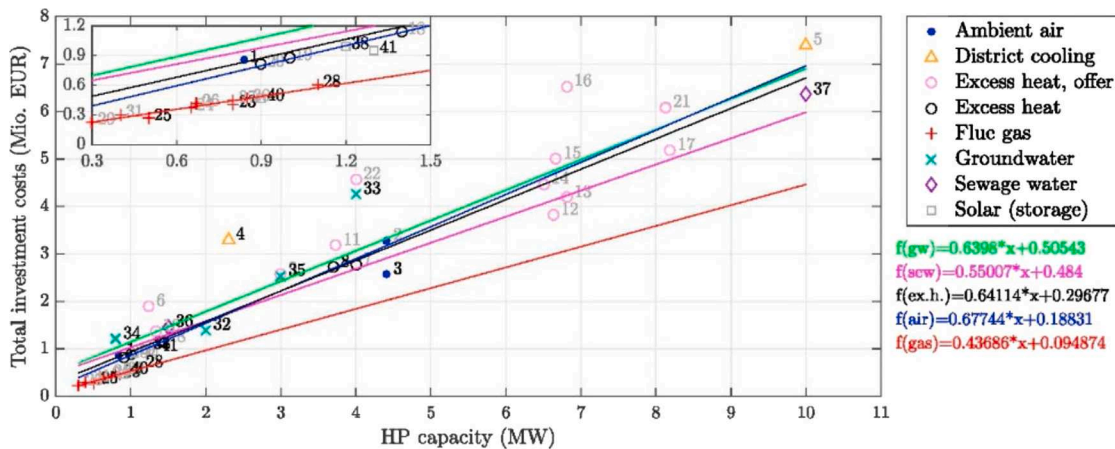


Fig. 12. Relationship of heat pump cost per MW.

A.4. Selection of COP

Fig. 13 shows the supply, return and COP achieved from large-scale european heat pump network schemes. The blue and orange indicate wether it is for cooling or heating.

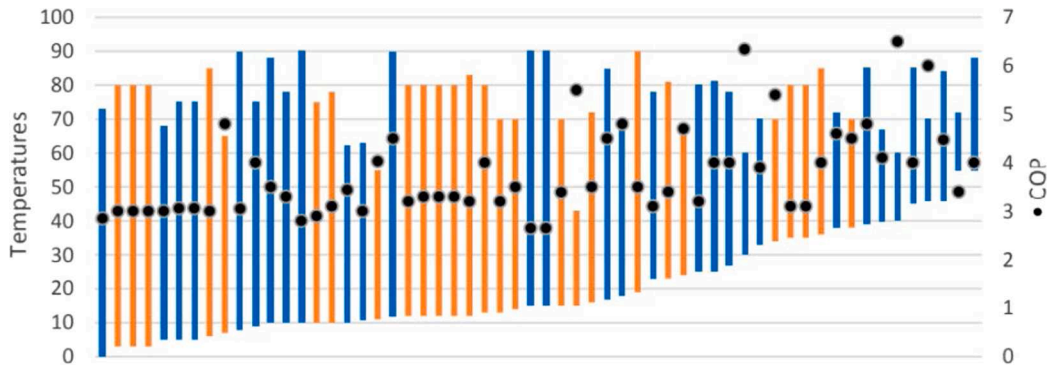


Fig. 13. Supply and return temperatures with associated COP.

A.5. Pipe sizing

Fig. 14 shows the relationship of nominal pipe diameter and the velocity of water and was used to size the pipes of each scenario of network.

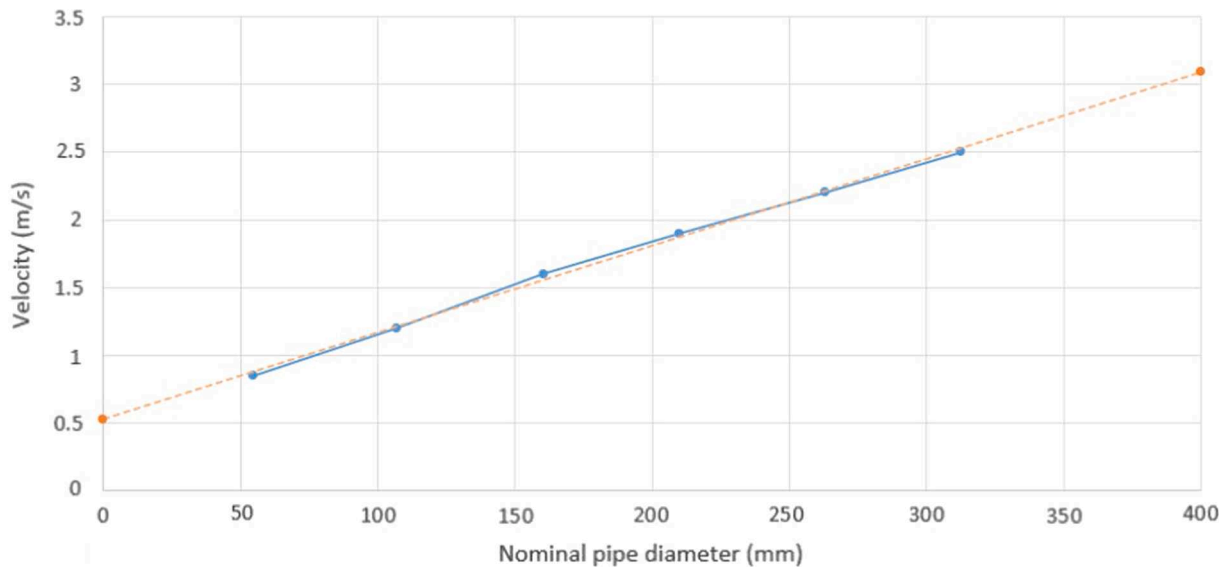


Fig. 14. Relationship of nominal pipe diameter and velocity of water.

References

- [1] BEIS. Net zero strategy: build back greener. Dep Business Energy Ind Strateg [Online]. Available: https://assets.publishing.service.gov.uk/government/uploads/system/uploads/attachment_data/file/1033990/net-zero-strategy-beis.pdf.
- [2] Commission E. Paris Agreement. [Online]. Available: https://ec.europa.eu/clima/eu-action/international-action-climate-change/climate-negotiations/paris-agreement_en.
- [3] L. Waters, Energy Consumption in the UK (ECUK.) [Online]. Available: https://assets.publishing.service.gov.uk/government/uploads/system/uploads/attachment_data/file/928350/2020_Energy_Consumption_in_the_UK_ECUK.pdf.
- [4] B.E.I.S., 2020 UK greenhouse gas emissions, provisional figures, Mar.
- [5] P.D. Lund, V. Arabzadeh, Modelling city-scale transient district heat demand by combining physical and data-driven approach, *Appl. Therm. Eng.* 178 (2020), <https://doi.org/10.1016/j.applthermaleng.2020.115590>.
- [6] M.-A. Millar, N. Burnside, Z. Yu, District heating challenges for the UK, *Energies* 12 (2) (Jan. 2019) 310, <https://doi.org/10.3390/en12020310>.
- [7] S. Kelly, M. Pollitt, An assessment of the present and future opportunities for combined heat and power with district heating (CHP-DH) in the United Kingdom, *Energy Policy* 38 (11) (Nov. 2010) 6936–6945, <https://doi.org/10.1016/j.enpol.2010.07.010>.
- [8] J. Cockroft, N. Kelly, A comparative assessment of future heat and power sources for the UK domestic sector, *Energy Convers. Manage* 47 (15–16) (Sep. 2006) 2349–2360, <https://doi.org/10.1016/j.enconman.2005.11.021>.
- [9] A.V. Olympios, et al., Delivering net-zero carbon heat: Technoeconomic and whole-system comparisons of domestic electricity- and hydrogen-driven technologies in the UK, *Energy Convers. Manage.* 262 (Jun. 2022) 115649, <https://doi.org/10.1016/j.enconman.2022.115649>.
- [10] H. Demir, M. Mobedi, S. Ülkü, A review on adsorption heat pump: problems and solutions, *Renew. Sustain. Energy Rev.* 12 (9) (Dec. 2008) 2381–2403, <https://doi.org/10.1016/j.rser.2007.06.005>.
- [11] D. Sarsentis, The heat pump installer gap: A lack of trained heat pump engineers will hamper green-home targets, 2022.
- [12] S. Werner, International review of district heating and cooling, *Energy* 137 617–631, doi: 10.1016/j.energy.2017.04.045.
- [13] UKGOV, Opportunity areas for district heating networks in the UK National Comprehensive Assessment of the potential for efficient heating and cooling. 2021.
- [14] M. Chaudry, M. Abeysekera, S.H.R. Hosseini, N. Jenkins, J. Wu, Uncertainties in decarbonising heat in the UK, *Energy Policy* 87 (2015) 623–640, <https://doi.org/10.1016/j.enpol.2015.07.019>.
- [15] K. Sartor, S. Quoilin, P. Dewallef, Simulation and optimization of a CHP biomass plant and district heating network, *Appl. Energy* 130 (Oct. 2014) 474–483, <https://doi.org/10.1016/j.apenergy.2014.01.097>.
- [16] B. Bach, J. Werling, T. Ommen, M. Münster, J.M. Morales, B. Elmegaard, Integration of large-scale heat pumps in the district heating systems of Greater Copenhagen, *Energy* 107 (Jul. 2016) 321–334, <https://doi.org/10.1016/j.energy.2016.04.029>.
- [17] X. Chen, et al., Heat loss optimization and economic evaluation of a new fourth generation district heating triple pipe system, *Appl. Therm. Eng.* 233 (Oct. 2023) 121160, <https://doi.org/10.1016/j.applthermaleng.2023.121160>.

- [18] M. Vesterlund, A. Toffolo, J. Dahl, Optimization of multi-source complex district heating network, a case study, *Energy* 126 (May 2017) 53–63, <https://doi.org/10.1016/j.energy.2017.03.018>.
- [19] E. Guelpa, Impact of network modelling in the analysis of district heating systems, *Energy* 213 118393, doi: 10.1016/J.ENERGY.2020.118393.
- [20] Department of Energy & Climate Change, Summary evidence on District Heating Networks in the UK.
- [21] T. Pregger, T. Naegler, W. Weimer-Jehle, S. Prehofer, W. Hauser, Moving towards socio-technical scenarios of the German energy transition—lessons learned from integrated energy scenario building, *Clim. Change* 162 (4) (Oct. 2020) 1743–1762, <https://doi.org/10.1007/s10584-019-02598-0>.
- [22] F. Giunta, S. Sawalha, Techno-economic analysis of heat recovery from supermarket's CO2 refrigeration systems to district heating networks, *Appl. Therm. Eng.* 193 (Jul. 2021) 117000, <https://doi.org/10.1016/j.applthermaleng.2021.117000>.
- [23] Z. Tian, B. Perers, S. Furbo, J. Fan, Thermo-economic optimization of a hybrid solar district heating plant with flat plate collectors and parabolic trough collectors in series, *Energy Convers. Manage.* 165 (Jun. 2018) 92–101, <https://doi.org/10.1016/j.enconman.2018.03.034>.
- [24] M. Capone, E. Guelpa, V. Verda, Optimal installation of heat pumps in large district heating networks, *Energies* 16 (3) (Feb. 2023) 1448, <https://doi.org/10.3390/en16031448>.
- [25] M. Münster, The role of district heating in the future Danish energy system, *Energy* 48(1) 47–55, doi: 10.1016/J.ENERGY.2012.06.011.
- [26] I. Pakere, M. Kacare, L. Murauskaitė, P. Huang, A. Volkova, Comparison of suitable business models for the 5th generation district heating system implementation through game theory approach, *Environ. Clim. Technol.* 27 (1) (2023) 1–15, <https://doi.org/10.2478/rtuect-2023-0001>.
- [27] S. Lavrijssen, B. Vitéz, Good Governance and the regulation of the district heating market, in: *Shaping an Inclusive Energy Transition*, Cham: Springer International Publishing, 2021, pp. 185–227.
- [28] U. Osis, N. Talcis, J. Ziemele, Challenges and barriers by transition towards 4th generation district heating system: a strategy to establish a pricing mechanism, *Latv. J. Phys. Tech. Sci.* 56 (4) (Aug. 2019) 17–37, <https://doi.org/10.2478/lpts-2019-0022>.
- [29] D. Quaggiotto, J. Vivian, A. Zarrella, Management of a district heating network using model predictive control with and without thermal storage, *Optim. Eng.* 22 (3) (Sep. 2021) 1897–1919, <https://doi.org/10.1007/s11081-021-09644-w>.
- [30] M. Brand, S. Svendsen, Renewable-based low-temperature district heating for existing buildings in various stages of refurbishment, *Energy* 62, 311–319, doi: 10.1016/J.ENERGY.2013.09.027.
- [31] Q. Qin, L. Gosselin, Multiobjective optimization and analysis of low-temperature district heating systems coupled with distributed heat pumps, *Appl. Therm. Eng.* 230 (Jul. 2023) 120818, <https://doi.org/10.1016/j.applthermaleng.2023.120818>.
- [32] P.A. Østergaard, B. V Mathiesen, B. Möller, H. Lund, A renewable energy scenario for Aalborg Municipality based on low-temperature geothermal heat, wind power and biomass, *Energy* 35(12) 4892–4901, doi: 10.1016/J.ENERGY.2010.08.041.
- [33] D. Hawkey, J. Webb, M. Winkler, Organisation and governance of urban energy systems: district heating and cooling in the UK, *J. Clean. Prod.* 50 (Jul. 2013) 22–31, <https://doi.org/10.1016/j.jclepro.2012.11.018>.
- [34] H. Lund, 4th Generation District Heating (4GDH). Integrating smart thermal grids into future sustainable energy systems, *Energy* 68, 1–11.
- [35] H. Dorotić, K. Čuljak, J. Miškić, T. Pukšec, N. Duić, Technical and economic assessment of supermarket and power substitution waste heat integration into existing district heating systems, *Energies* 15 (5) (Feb. 2022) 1666, <https://doi.org/10.3390/en15051666>.
- [36] H. Kauko, D. Rohde, A. Hafner, Local heating networks with waste heat utilization: low or medium temperature supply? *Energies* 13 (4) (Feb. 2020) 954, <https://doi.org/10.3390/en13040954>.
- [37] W. Gao, S. Masum, M. Qadrdan, H.R. Thomas, Estimation and prediction of shallow ground source heat resources subjected to complex soil and atmospheric boundary conditions, *Renew. Energy* 197 (2022) 978–994, <https://doi.org/10.1016/j.renene.2022.07.148>.
- [38] A. Lane, How flooded coal mines could heat homes, 2021.
- [39] J. Perez Silva, C. McDermott, A. Fraser-Harris, The value of a hole in coal: assessment of seasonal thermal energy storage and recovery in flooded coal mines, *Earth Sci. Syst. Soc.* 2 (Mar. 2022), <https://doi.org/10.3389/esss.2022.10044>.
- [40] The Coal Authority, Mine Water Heat, *GOV.UK*, [Online]. Available: <https://www.gov.uk/government/collections/mine-water-heat>.
- [41] J. Keirstead, M. Jennings, A. Sivakumar, A review of urban energy system models: approaches, challenges and opportunities, *Renew. Sustain. Energy Rev.* 16 (6) (2012) 3847–3866, <https://doi.org/10.1016/j.rser.2012.02.047>.
- [42] M.-A. Millar, B. Elrick, G. Jones, Z. Yu, N.M. Burnside, Roadblocks to low temperature district heating, *Energies* 13 (22) (2020) 5893, <https://doi.org/10.3390/en13225893>.
- [43] The Coal Authority, Geothermal energy from abandoned coal mines - Coal Authority. [Online]. Available: <https://www2.groundstability.com/geothermal-energy-from-abandoned-coal-mines/>.
- [44] M. Vokurka, A. Kunz, Case study of using the geothermal potential of mine water for central district heating—The Rožná Deposit, Czech Republic, *Sustainability* 14 (4) (Feb. 2022) 2016, <https://doi.org/10.3390/su14042016>.
- [45] E. Peralta Ramos, K. Breede, G. Falcone, Geothermal heat recovery from abandoned mines: a systematic review of projects implemented worldwide and a methodology for screening new projects, *Environ. Earth Sci.* 73 (11) (Jun. 2015) 6783–6795, <https://doi.org/10.1007/s12665-015-4285-y>.
- [46] A. Matas-Escamilla, et al., Mine water as a source of energy: an application in a coalfield in Laciana Valley (León, NW Spain), *Clean Technol. Environ. Policy* (May 2023), <https://doi.org/10.1007/s10098-023-02526-y>.
- [47] H. Fang, J. Xia, K. Zhu, Y. Su, Y. Jiang, “Industrial waste heat utilization for low temperature district heating,” *Energy Policy*, vol. 62, pp. 236–246, doi: 10.1016/J.ENPOL.2013.06.104.
- [48] E. Guelpa, C. Toro, A. Sciacovelli, R. Melli, E. Sciubba, V. Verda, Optimal operation of large district heating networks through fast fluid-dynamic simulation, *Energy* 102 (May 2016) 586–595, <https://doi.org/10.1016/j.energy.2016.02.058>.
- [49] S. Werner, District heating and cooling in Sweden, *Energy* 126 (2017) 419–429, <https://doi.org/10.1016/J.ENERGY.2017.03.052>.
- [50] Ramboll, “Bunhill 2 District Heating Network - Heating up London,” Islington, London. [Online]. Available: <https://uk.ramboll.com/projects/ruk/heating-up-london>.
- [51] M. Santin, D. Chinese, A. De Angelis, M. Biberacher, Feasibility limits of using low-grade industrial waste heat in symbiotic district heating and cooling networks, *Clean Technol. Environ. Policy* 22 (6) (Aug. 2020) 1339–1357, <https://doi.org/10.1007/s10098-020-01875-2>.
- [52] K.N. Finney, et al., Modelling and mapping sustainable heating for cities, *Appl. Therm. Eng.* 53 (2) (May 2013) 246–255, <https://doi.org/10.1016/j.applthermaleng.2012.04.009>.
- [53] A. Ashfaq, A. Ianakiev, Cost-minimised design of a highly renewable heating network for fossil-free future, *Energy* 152 (Jun. 2018) 613–626, <https://doi.org/10.1016/j.energy.2018.03.155>.
- [54] A. Atienza-Márquez, J.C. Bruno, A. Coronas, Recovery and transport of industrial waste heat for their use in urban district heating and cooling networks using absorption systems, *Appl. Sci.* 10 (1) (Dec. 2019) 291, <https://doi.org/10.3390/app10010291>.
- [55] T. A. Company, “No Title.” 2019, [Online]. Available: <https://www.anylogic.com>.
- [56] E. Guelpa, A. Sciacovelli, V. Verda, Thermo-Fluid Dynamic Model of Complex District Heating Networks for the Analysis of Peak Load Reductions in the Thermal Plants 2015, doi: 10.1115/IMECE2015-52315.
- [57] J. Duquette, A. Rowe, P. Wild, Thermal performance of a steady state physical pipe model for simulating district heating grids with variable flow, *Appl. Energy* 178 (Sep. 2016) 383–393, <https://doi.org/10.1016/j.apenergy.2016.06.092>.
- [58] G. Rogers, Y. Mayhew, *Engineering Thermodynamics: Work and Heat Transfer*, Longman Scientific, 1992.
- [59] Q. Meng, M. Mourshed, Degree-day based non-domestic building energy analytics and modelling should use building and type specific base temperatures, *Energy Build.* 155 (Nov. 2017) 260–268, <https://doi.org/10.1016/j.enbuild.2017.09.034>.
- [60] RAPID-HPC, FINAL REPORT ON ANALYSIS OF HEAT PUMP DATA FROM THE RENEWABLE HEAT PREMIUM PAYMENT (RHPP) SCHEME, 2017.
- [61] Centre for Environmental Data Analysis, Met Office MIDAS Open, ceda.ac.uk, 2018.
- [62] A. O'Mahoney, Review of Typical Domestic Consumption Values 2021. [Online]. Available: <https://www.ofgem.gov.uk/publications/review-typical-domestic-consumption-values-2021>.
- [63] X. Liu, J. Wu, N. Jenkins, A. Bagdanavicius, Combined analysis of electricity and heat networks, *Appl. Energy* 162 (2016) 1238–1250, <https://doi.org/10.1016/j.apenergy.2015.01.102>.
- [64] E. C. for Standardization, “EN 13480-1:2017 - Metallic industrial piping,” 2017. [Online]. Available: <https://standards.iteh.ai/catalog/standards/cen/bd84850d3-f8bf-46aa-b124-76647db08ff7/en-13480-1-2017>.
- [65] OpenStreetMap, “OpenStreetMap, openstreetmap.org, 2023.
- [66] M. Chung, P.-S. Jung, R.H. Rangel, Semi-analytical solution for heat transfer from a buried pipe with convection on the exposed surface, *Int. J. Heat Mass Transf.* 42 (20) (Oct. 1999) 3771–3786, [https://doi.org/10.1016/S0017-9310\(99\)00046-0](https://doi.org/10.1016/S0017-9310(99)00046-0).
- [67] *Hydraulics of Open Channel Flow*. Elsevier, 2004.
- [68] *The Engineering Toolbox*, Power Gained by Fluid from Pump or Fan, engineeringtoolbox.com, 2004.
- [69] B.E.I.S., Greenhouse gas reporting: conversion factors 2020 - GOV.UK, Jun, [Online]. Available: https://assets.publishing.service.gov.uk/government/uploads/system/uploads/attachment_data/file/891105/Conversion_Factors_2020_-_Condensed_set_for_most_users_.xlsx.
- [70] B. Group, The Government's Standard Assessment Procedure for Energy Rating of Dwellings Version 10.2, 2022.
- [71] H. Pieper, T. Ommen, F. Buhler, B.L. Paaske, B. Elmgaard, W.B. Markussen, Allocation of investment costs for large-scale heat pumps supplying district heating, *Energy Procedia* 147 (Aug. 2018) 358–367, <https://doi.org/10.1016/j.egypro.2018.07.104>.
- [72] HOMER Energy LLC, “Real discount rate,” homenergy.com.
- [73] Introduction to the Mathematics of Finance. Elsevier, 2013.
- [74] Y. Cui, et al., Techno-economic assessment of the horizontal geothermal heat pump systems: a comprehensive review, *Energy Convers. Manage.* 191 (Jul. 2019) 208–236, <https://doi.org/10.1016/j.enconman.2019.04.018>.
- [75] Met Office, MIDAS Open: UK daily temperature data, v202107, NERC EDS Centre for Environmental Data Analysis, 2021. [Online]. Available: <https://doi.org/10.5285/92e823b277cc4f439803a87f5246db5f>.
- [76] F. Guo, X. Zhu, J. Zhang, X. Yang, Large-scale living laboratory of seasonal borehole thermal energy storage system for urban district heating, *Appl. Energy* 264 (2020) 114763, <https://doi.org/10.1016/j.apenergy.2020.114763>.
- [77] Interactive Map Viewer | Coal Authority. [Online]. Available: <https://mapapps2.bgs.ac.uk/coalauthority/home.html>.
- [78] A. David, B.V. Mathiesen, H. Aeverfalk, S. Werner, H. Lund, Heat roadmap europe: large-scale electric heat pumps in district heating systems, *Energies* 10 (4) (Apr. 2017) 578, <https://doi.org/10.3390/en10040578>.

- [79] ETSAP, District Heating. IEA-ETSAP Technology Brief E16, IEA ETSAP - Technol. Br., no. January, p. 7, 2013.
- [80] U. K. Emissions, T. Scheme, U. K. Ets, I. Strategy, Participating in the UK ETS, 2022, pp. 1–12.
- [81] H.M. Treasury, *The Green Book Central Government Guidance on Appraisal*, Open Government Licence, London, 2022.
- [82] F. I. N. T. H. E. R. M. a.s, “Pre-insulated pipes and accessories catalogue.” [Online]. Available: https://www.fintherm.cz/downloads/pre_insulated_pipes_catalogue_fintherm_en_2019_07.pdf.
- [83] “Heat Networks: Code of Practice for the UK,” 2014. [Online]. Available: https://www.heatweb.co.uk/w/images/4/49/Heat-Networks-Code-of-Practice-for-the-UK_draft_consultation.pdf.
- [84] M. Fox, *email conversation*, Barnsley Council (2022).
- [85] J. Fitó, J. Ramousse, S. Hodencq, F. Wurtz, Energy, exergy, economic and exergoeconomic (4E) multicriteria analysis of an industrial waste heat valorization system through district heating, *Sustain. Energy Technol. Assessments* 42 (Dec. 2020) 100894, <https://doi.org/10.1016/j.seta.2020.100894>.
- [86] Element Energy, “The potential for recovering and using surplus heat from industry,” 2014. [Online]. Available: https://assets.publishing.service.gov.uk/government/uploads/system/uploads/attachment_data/file/294901/element_energy_et_al_potential_for_recovering_and_using_surplus_heat_from_industry_appendix.pdf.
- [87] “Barnsley Zero Carbon Sustainable Energy Action Plan (SEAP),” 2020.
- [88] T. Economics, Uk Natural Gas, 2022. <https://tradingeconomics.com/commodity/uk-natural-gas>.
- [89] IEA, Levelized cost of heating (LCOH) for consumers, for selected space and water heating technologies and countries, 2021. <https://www.iea.org/data-and-statistics/charts/levelized-cost-of-heating-lcoh-for-consumers-for-selected-space-and-water-heating-technologies-and-countries>.
- [90] postcodesbyaddress, Find all postcodes, streets and places across the UK - Postcode by address. [Online]. Available: <https://postcodebyaddress.co.uk/>.
- [91] Department for Levelling Up Housing and Communities, Energy Performance of Buildings Certificates, EPC Databases, [Online]. Available: <https://www.gov.uk/government/statistical-data-sets/live-tables-on-energy-performance-of-buildings-certificates>.
- [92] PipeFlow, Pipe Friction Factor Calculation. [Online]. Available: <https://www.pipeflow.com/pipe-pressure-drop-calculations/pipe-friction-factors>.
- [93] The Engineering Toolbox, “Prandtl Number,” *engineeringtoolbox.com*.
- [94] nuclear-power.com, “Nusselt Number | Definition, Formula & Calculation,” *nuclear-power.com*.